



UNIVERSITEIT•STELLENBOSCH•UNIVERSITY
jou kennisvennoot • your knowledge partner

MEng Title

Johann Ruben van Tonder
22569596

Thesis presented in partial fulfilment of the requirements for the degree of Master of Engineering (Electronic) in the Faculty of Engineering at Stellenbosch University

Supervisor:

November 2022

Acknowledgements

I would like to sincerely thank the following people for assisting me in the completion of my project:



UNIVERSITEIT•STELLENBOSCH•UNIVERSITY
jou kennisvennoot • your knowledge partner

Plagiaatverklaring / Plagiarism Declaration

1. Plagiaat is die oorneem en gebruik van die idees, materiaal en ander intellektuele eiendom van ander persone asof dit jou eie werk is.

Plagiarism is the use of ideas, material and other intellectual property of another's work and to present it as my own.

2. Ek erken dat die pleeg van plagiaat 'n strafbare oortreding is aangesien dit 'n vorm van diefstal is.

I agree that plagiarism is a punishable offence because it constitutes theft.

3. Ek verstaan ook dat direkte vertalings plagiaat is.

I also understand that direct translations are plagiarism.

4. Dienooreenkomsdig is alle aanhalings en bydraes vanuit enige bron (ingesluit die internet) volledig verwys (erken). Ek erken dat die woordelikse aanhaal van teks sonder aanhalingstekens (selfs al word die bron volledig erken) plagiaat is.

Accordingly all quotations and contributions from any source whatsoever (including the internet) have been cited fully. I understand that the reproduction of text without quotation marks (even when the source is cited) is plagiarism

5. Ek verklaar dat die werk in hierdie skryfstuk vervat, behalwe waar anders aangedui, my eie oorspronklike werk is en dat ek dit nie vantevore in die geheel of gedeeltelik ingehandig het vir bepunting in hierdie module/werkstuk of 'n ander module/werkstuk nie.

I declare that the work contained in this assignment, except where otherwise stated, is my original work and that I have not previously (in its entirety or in part) submitted it for grading in this module/assignment or another module/assignment.

22569596	
Studentenommer / Student number	Handtekening / Signature
J.R. van Tonder	April 22, 2023
Voorletters en van / Initials and surname	Datum / Date

Abstract

English

Afrikaans

Contents

Declaration	ii
Abstract	iii
List of Figures	vii
List of Tables	ix
Nomenclature	x
1. Introduction	1
1.1. Background	1
1.2. Problem Statement	1
1.3. Summary of Work	1
1.4. Scope	1
1.5. Format of Report	1
2. Literature Review	2
2.1. Related work on USV's	2
2.1.1. South Africa Sailboat	2
2.1.2. Italy Sailboat	3
2.1.3. Norwegian Sailboat	4
2.1.4. Sweden Sailboat	5
2.2. Control techniques for USV's	6
2.2.1. Rudder Control	6
2.2.2. Sail Control	9
2.3. Platform development of USV	9
2.4. Usages of USV	11
3. Modeling of Ocean Vessels	13
3.1. Standard Ocean Vessel Notation	13
3.2. Kinematics	14
3.3. Kinetics	15
3.4. Hydrodynamic Forces and Moments	16
3.5. Restoring Forces and Moments	17

3.6.	Environmental Disturbances	19
3.6.1.	Current-induced Forces and Moments	19
3.6.2.	Wave-induced Forces and Moments	19
3.6.3.	Wind-induced Forces and Moments	20
3.7.	Simplifications of 6-DOF	21
3.7.1.	Standard 3-DOF Horizontal Model	21
3.7.2.	Simplified 3-DOF Horizontal Model	22
3.8.	Summary	23
3.9.	Simulation Results	24
4.	Modeling of a Fixed-Wing Sail, Keel and Rudder	25
4.1.	Rudder Theory	25
4.1.1.	Rudder Theory and Terminology	25
4.1.2.	Hydrodynamics of a Rudder	25
4.1.3.	Rudder Forces and Moments	26
4.2.	Sail Theory	27
4.2.1.	Sail Theory and Terminology	27
4.2.2.	Aerodynamics of a Sail	29
4.2.3.	Sail Forces and Moments	31
5.	Guidance and Waypoint Navigation	35
5.1.	Guidance System	35
5.2.	Straight path Generation based on Waypoints	37
5.3.	Line-of-Sight (LOS) Steering Law	38
5.4.	Path-Following Controllers	40
5.5.	Circle of Acceptance for Surface Vessel	41
6.	Fundamental Properties of Linear steering dynamic model	42
6.1.	Ship Steering Dynamics Model Reduction	42
6.2.	First Order Nomoto Model	44
6.3.	Second Order Nomoto Model	45
6.4.	Conclusion	47
7.	Control of USV	49
7.1.	Ocean Vessel Steering Control	49
7.1.1.	Linear Rudder Control	52
7.1.2.	Non-Linear Rudder Control	55
7.2.	Ocean Vessel Propulsion Control	57
7.3.	Maneuverability Control	60
Bibliography		62

A. Additional Modelling Information	64
A.1. Notation and Vector Definitions	64
A.2. Modeling Equations	65

List of Figures

2.1. UCT Sailboat	2
2.2. Variable draft sailing spar	3
2.3. Aeolus, sailing boat of ETH Zurich	4
2.4. Sailboat used for modeling	5
2.5. Sailboat provided by University of Hong Kong	5
2.6. Reference heading α^* , obtained angle α and rudder input δ	7
2.7. Raw and average wind direction σ raw and σ avg, heading ψ and course over ground X	7
2.8. Rule based controller for sail	9
2.9. Platform developed by UCT sailboat	10
2.10. GUI developed for sailboat monitoring	11
2.11. Saildrone's USV	11
2.12. Routes of the USV's in Arctic Mission	12
3.1. Motion variables for an ocean vessel	13
3.2. Transverse metacentric stability	17
3.3. Ocean vessel's heading angle	20
3.4. Wind angle on vessel	20
3.5. Standard 3-DOF Horizontal Model	21
3.6. Forces caused by waves in x- and y-direction	24
4.1. Terminology of a lifting foil	25
4.2. Pressure around the rudder	26
4.3. Lift and drag force on rudder	26
4.4. Definition of Rudder Angles	27
4.5. Naming convention of a sail	28
4.6. Terminology of a sail wing and shape	28
4.7. Windward and leeward definitions	29
4.8. Flow field without circulation	29
4.9. Superposition of circulation and non-circulation solution to give lift	30
4.10. Lift and drag forces due to wind on sail wing	30
4.11. Lift force component represented as a power curve	33
5.1. Ground track between source waypoint and destination waypoint	35

5.2.	Cross-track error and in-track distance along track	36
5.3.	Guidance Axis System	36
5.4.	Straight lines and circular arc segments for waypoint guidance	38
5.5.	LOS guidance where the desired course angle x_d is chosen to point toward the LOS intersection point (x_{los}, y_{los})	39
5.6.	Circle of acceptance with constant radius R	39
5.7.	LOS guidance principle where the side slip angle B can be applied and compensated for by using integral action	41
6.1.	Sway-yaw-roll motion coordinate system	42
6.2.	First Order bode Plot	48
6.3.	Second Order Bode Plot	48
6.4.	Fourth Order Bode Plot	48
7.1.	Reference angles of sailboat	49
7.2.	Root locus of first order system	51
7.3.	Corrected root locus of first order system	52
7.4.	Bode plot	53
7.5.	Step response of first order system	53
7.6.	Simulink model of system	54
7.7.	Closed loop step response	54
7.8.	Implementation of controller in fourth order transfer function	55
7.9.	Comparison between 1st order and 4th order step responses	55
7.10.	Linear control of heading	56
7.11.	Non-Linear control of heading	56
7.12.	Linear control of heading	56
7.13.	Non-Linear control of heading	57
7.14.	Sail Angle for Apparent wind angle of 90°	58
7.15.	Optimal sail angle for varying wind angle	58
7.16.	Sail force for specific apparent wind angles	59
7.17.	Boat Speed with a AWV of 5 km.s^{-1}	60
7.18.	No-go zone	60
7.19.	Tacking	61

List of Tables

A.1. SNAME Notation for ocean vessels	64
A.2. Rigid body motion vectors	64
A.3. Sail Angle Look-up Table	66

Nomenclature

Ocean Vessel Dynamics

X, Y, Z	Coordinates of force vector decomposed in the body-fixed frame(surge, sway and heave forces)
K, M, N	Coordinates of moment vector decomposed in the body-fixed frame(roll, pitch and yaw moment)
u, v, w	Coordinates of linear velocity vector decomposed in the body-fixed frame(surge, sway and heave velocities)
p, q, r	Coordinates of angular velocity vector decomposed in the body-fixed frame(roll, pitch and yaw angular velocities)
x, y, z	Coordinates of position vector decomposed in the body-fixed frame(surge, sway and heave positions)
ϕ, θ, ψ	Coordinates of Euler angle vector decomposed in the body-fixed frame(roll, pitch and yaw Euler angles)

Guidance and Navigation

x_i, y_i, ψ_i	Coordinate system for guidance control known as the <i>pose</i>
$\psi_{heading}$	Track heading
L_{track}	Track length
(E_{src}, N_{src})	Source Waypoint
(E_{dest}, N_{dest})	Destination Waypoint

Acronyms and abbreviations

SNAME	Society of Naval Architects and Engineers
CG	Centre of gravity of a vessel
CB	Centre of buoyancy of a vessel
AoA	Angle of attack
Re	Reynolds number
USV	Unmanned Surface Vehicle
AWA	Apparent Wind Angle
AWV	Apparent Wind Velocity

Sailing Terminology

Bow	Front of the sailboat
Stern	Rear of the sailboat
Luff	Leading edge of the sail
Leech	Trailing edge of the sail
Foot	Bottom edge of the sail
Boom	Attached point of the foot to the sailboat
Clew	Attachment point of the leech
Tack	Attachment point of the luff
Chord	Straight line between leading and trailing edge
Camber	Perpendicular distance from the chord line to the foil
Draft	Position of the maximum camber along the chord line
Entry	Angle of the leading edge to the chord line
Exit	Angle of the trailing edge to the chord line
AoA	Angle between oncoming flow and the chord line
Twist	Angle between the chord line and the sailboat's centre line

Chapter 1

Introduction

1.1. Background

1.2. Problem Statement

The problem is that of modeling and controlling a fixed wing unmanned surface vehicle(USV), or in layman's terms a sailboat. Control strategies and techniques are applied to find the best way of controlling a USV on a line trajectory and performing speed control.

1.3. Summary of Work

1.4. Scope

1.5. Format of Report

Chapter 2

Literature Review

In recent years the development of robotics has enabled a new era of exploration. This exploration is made possible through USV's, more commonly known as sailboats. Sailboats can be used to explore area's of the ocean previously unexplored. The sailboat are equipped with an array of sensors that collect data on important ocean factors and the ecosystem inside. This chapter will review the usage of sailboats to collect data and exploration usages. Also it will look into the control techniques used in sailboats and how a sailboat is controlled to stay on the designated course.

2.1. Related work on USV's

2.1.1. South Africa Sailboat



Figure 2.1: UCT Sailboat

The first sailboat used for review is close to home. The sailboat was developed by the University of Cape Town(UCT) [1], the sailboat is illustrated in Figure 2.1. The study focussed on modeling and simulation of a sailboat. No sort of control techniques was

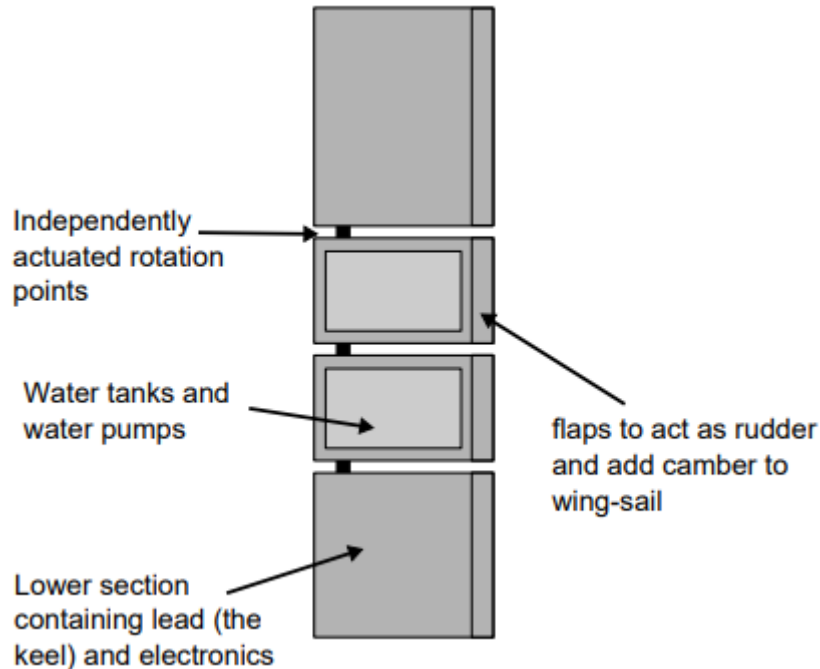


Figure 2.2: Variable draft sailing spar

developed. The modelling of the sailboat was done in the three and four degrees of freedom, which is the most popular degrees of freedom when considering sailboats. The four degrees of freedom are surge, sway, yaw and roll. The field tests collected valuable data which agreed with the limitations mentioned in the study. The study used a fixed wing sail but also proposed a novel sail trimming on a fixed wing sail. The platform that was developed to monitor the sailboat performed well in field test but their was one problem with the wind sensor not giving reliable data. The field tests were executed on dams near UCT.

2.1.2. Italy Sailboat

Now lets move over to Europe, more specifically Italy and the University of Pisa with Aeolus [2]. Aeolus is a small model sized sailing boat, provided by ETH Zurich, fitted with a wind sensor. The sailboat makes use of a fabric sail unlike the sailboat illustrated in Figure 2.1. Aeolus makes use of a main sail and a jib. The sail controller is only used to adjust the main sail angle.



Figure 2.3: Aeolus, sailing boat of ETH Zurich

The study focussed on developing navigation and control strategies for an autonomous sailing model boat. In the study different rudder controllers were implemented to perform the maneuvering technique called tacking and performed field test in the lake Zurich, Switzerland. The study successfully implemented a turning dynamic, real time data collecting and filtering, sailing upwind and executing tack maneuvers.

2.1.3. Norwegian Sailboat

Not far from Zurich lies the ancestors of the vikings who mastered the arts of sailing. The Norwegian model [3] was based on the sailboat illustrated in Figure 2.4. The thesis focused on modeling, simulation and control of a sailboat. The study first developed a mathematical model in four degrees of freedom. From this mathematical model the rudder and sail controller was designed. New strategies for a course control and a technique to reduce roll motion was also developed. A path following strategy was created and state estimation through sensors was created. All of the above mentioned controllers and strategies was tested and achieved desirable results.



Figure 2.4: Sailboat used for modeling

2.1.4. Sweden Sailboat



Figure 2.5: Sailboat provided by University of Hong Kong

The study focused on developing a mathematical model with simulations of the control strategies. The control was designed for optimal trajectory approach. The tests were confined to indoor test where fans were used to generate wind. The fans caused turbulence which impacted the tests. The modeling did not take into consideration the roll, pitch and heave and the control strategies still performed accurately. The controllers implemented were a PD controller and the force polar diagram for the sail angle.

2.2. Control techniques for USV's

The control of a USV is a problem of steering the vehicle in the appropriate direction and controlling the sail angle. The two common sails used are either a tradition fabric sail [4] or a fixed wing sail [5]. The steering of a vehicle is made possible through controlling the rudder. A USV is known as a underactuated vessel, which is when a vehicle has uncontrollable states. The only controllable states are the yaw rate and surge speed, which is defined in Section 3.

2.2.1. Rudder Control

The sailboat made use of a basic rudder control, which did not achieve desirable results. The controller used to control the rudder is a lead controller***expand***, although their was reported that it performed badly due to amplifying the high frequency noise. The study concluded that there is still significant amount of work required on the rudder control.

Aeolus makes use of two rudder controllers either using the one or the other depending on the circumstance. When the error signal e , which is the difference between the desired heading and the actual heading, is small the controller is defined as

$$\delta = k_p e \quad (2.1)$$

this is a simple Proportional controller for the rudder at small error signals. The second controller is used in the case of the error signal being large when implementing a non-linear controller. The non-linear controller defines a nonlinear gain $k(e)$ as

$$k(e) = \frac{k_p}{1 + c_p |e|} \quad (2.2)$$

The constant c_p is used to tune the control action when the error is large. This enables the sailboat to perform special maneuvering called tacking. The performance of the rudder controller is illustrated in Figure 2.6 and 2.7. The rudder controller performed reasonably accurate apart from suffering from drift which causes a difference in the heading ψ and course over ground X .

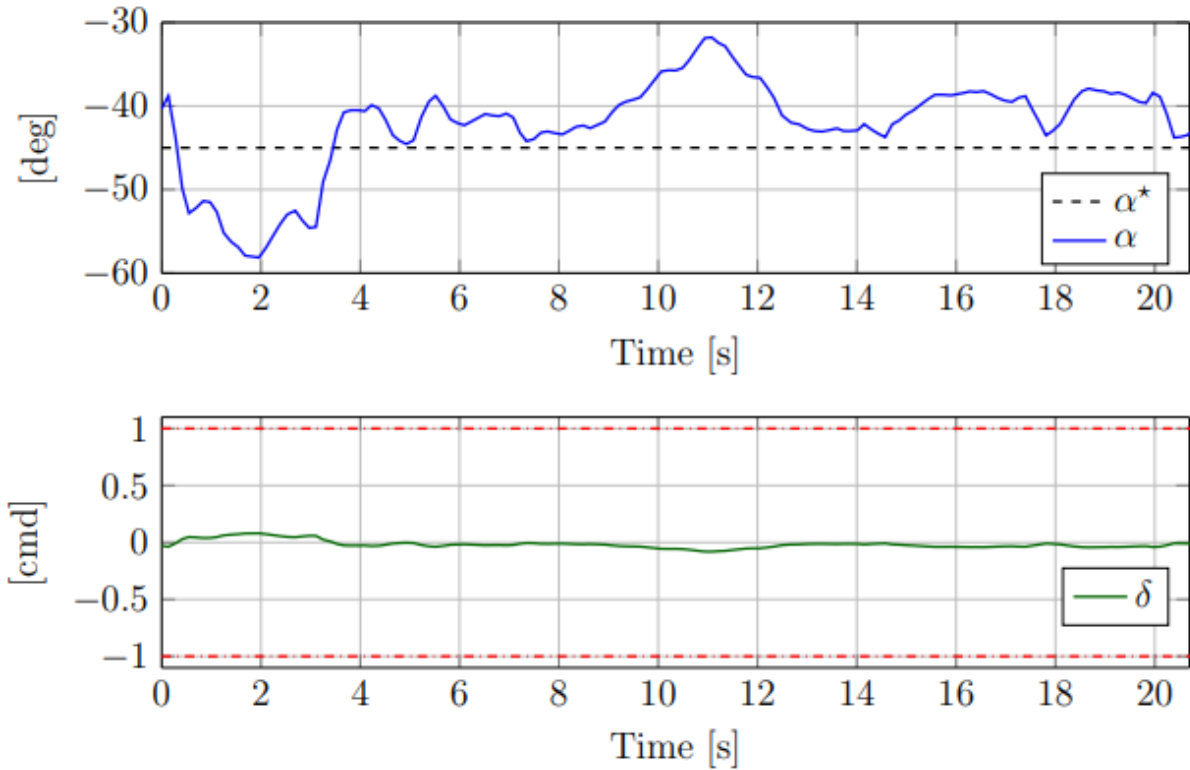


Figure 2.6: Reference heading α^* , obtained angle α and rudder input δ

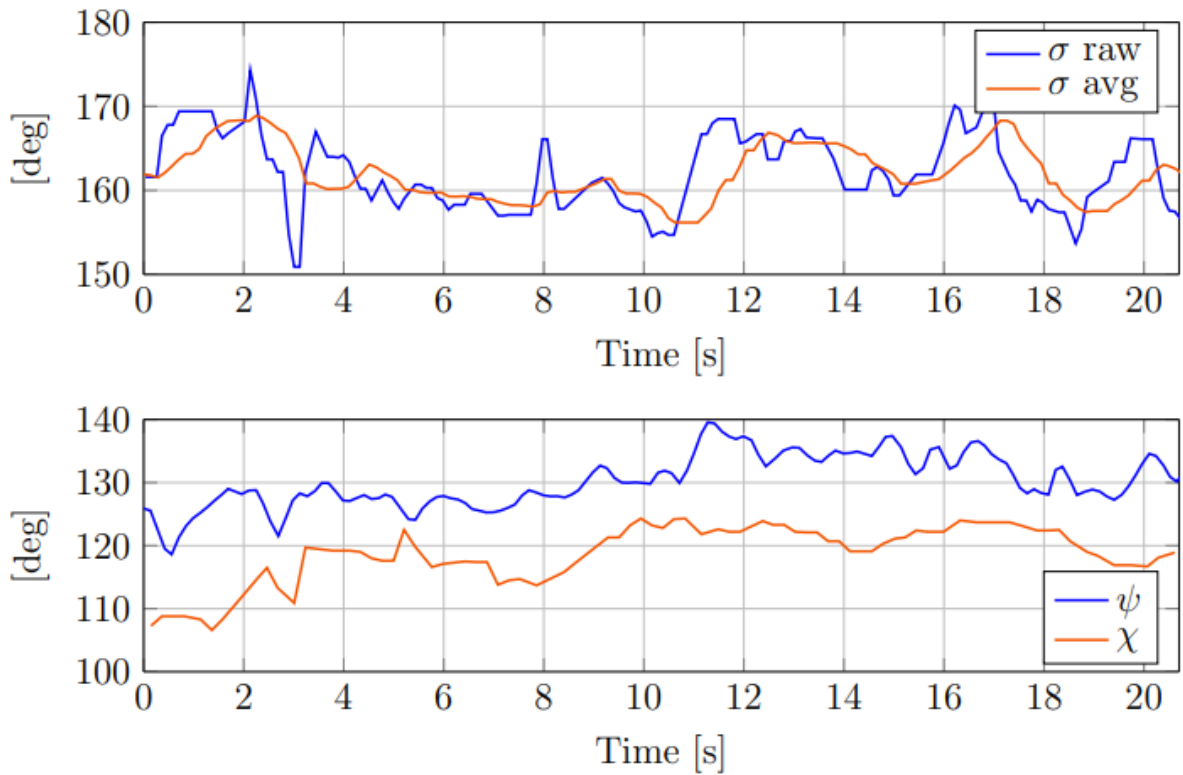


Figure 2.7: Raw and average wind direction σ raw and σ avg, heading ψ and course over ground X

The rudder control of the Norwegian sailboat is by far the most complex discussed thus

far, the controller is using control Lyapunov functions and a recursive design approach. Where the new state variables are,

$$z_1 = \psi + \beta_b + X_d \quad (2.3)$$

and

$$z_2 = r - \alpha \quad (2.4)$$

where X_d is the desired heading, z_1 is the error from the desired course angle, ψ is the actual heading and β_b is the necessary drift angle such that the desired course angle is achieved. β_b is a bias, the drift and course angle is defined as

$$\beta = \arctan2(v\cos(\phi), u) \quad (2.5)$$

$$X = \psi + \beta \quad (2.6)$$

The goal of the controller is to make the Lyapunov Function stable,

$$\dot{V}_1 = -K_p z_1^2 + z_1 z_2 \quad (2.7)$$

Solving the controller action u results in the state z_1 to due the following procedure,

$$z_1 = \text{mod}(z_1 + \pi, 2\pi) - \pi \quad (2.8)$$

where mod is the modulo operation. This ensures that the boat always turns in the direction that has the smallest error. If one calculates z_1 one will always end up tacking up-wind an jibing down-wind. The correction term β_b is used to compensate for the drift angle, by using a lookup-table that stores the necessary drift angles to keep a desired course. A simpler method was introduced in this study, where z_1 state of a traditional heading controller is equal to

$$z_1 = \psi - \psi_d = \psi - (X_d - \beta_b) = \psi + \beta_d - X_d \quad (2.9)$$

The study found the following solution for β_b as follows

$$\beta_b = -\alpha_k \cos(\phi) \quad (2.10)$$

where

$$\alpha_k = -\frac{\beta}{\cos(\phi)} \quad (2.11)$$

The lift the rudder can create is limited which limits the maximum moment can create in yaw. The controller does not take this into account and therefore to smooth the rudder

response a second order low-pass filter was added. The transfer function is shown below,

$$F(s) = \frac{\omega^2}{s^2 + 2\omega + \omega^2} \quad (2.12)$$

where $T_\psi = \frac{1}{\omega}$ was treated as the tuning parameter.

2.2.2. Sail Control

The sailboat of the UCT sailboat was controlled by setting the sail angle of attack to a predetermined angle depending on the apparent wind angle. The apparent wind angle was divided into three regions $-90 < \beta < 90$, $-160 < \beta < 160$ and $-180 < \beta < 180$.

The hardware on the ETH Zurich sailboat platform did not allow for feedback measurements of the position of the sail and therefore a simple open loop controller was implemented. The controller was based on a rule, the closer Aeolus is sailing opposite the wind direction, that is closer to 0° , the more the sail is closed. The rule based controller is shown in Figure 2.8. The parameters x_1 and x_2 can be changed at run time and the higher the sail command μ , the more the sail is closed.

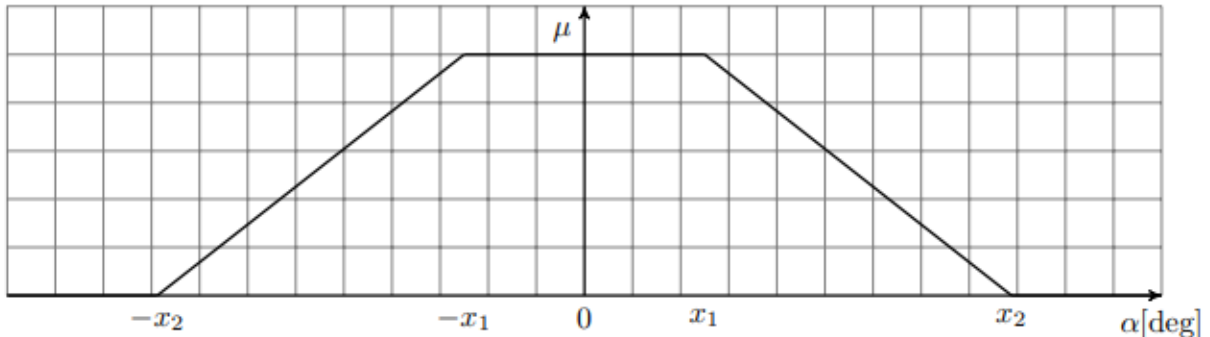


Figure 2.8: Rule based controller for sail

To obtain the optimal sail angle to give the highest forward acceleration for a given wind direction, making λ_d , which is the sail angle, a function of β_{ws} , $\lambda_d(\beta_{ws})$. This was achieved by defining a function independent of wind speed and measuring the force it generates. The optimal sail angle was stored in a look-up table, taking into account the restriction of possible sailing angles depending on the wind direction.

2.3. Platform development of USV

The platform required for sailboat control is quite simple. It requires a rudder angle feedback, compass or gyro, wind sensor, GPS sensor and the methods for controlling the sail and rudder. Accompanying these sensors onboard an off board station is required to monitor the sailboat's state. The difficulty in designing and implementing the platform is

the limitation of space available on the model sized sailboats. The goal of these small scale sailboats are to test control strategies for navigation and route planning. It is very seldom that you would add any other sensors apart from cameras used for obstacle avoidance.

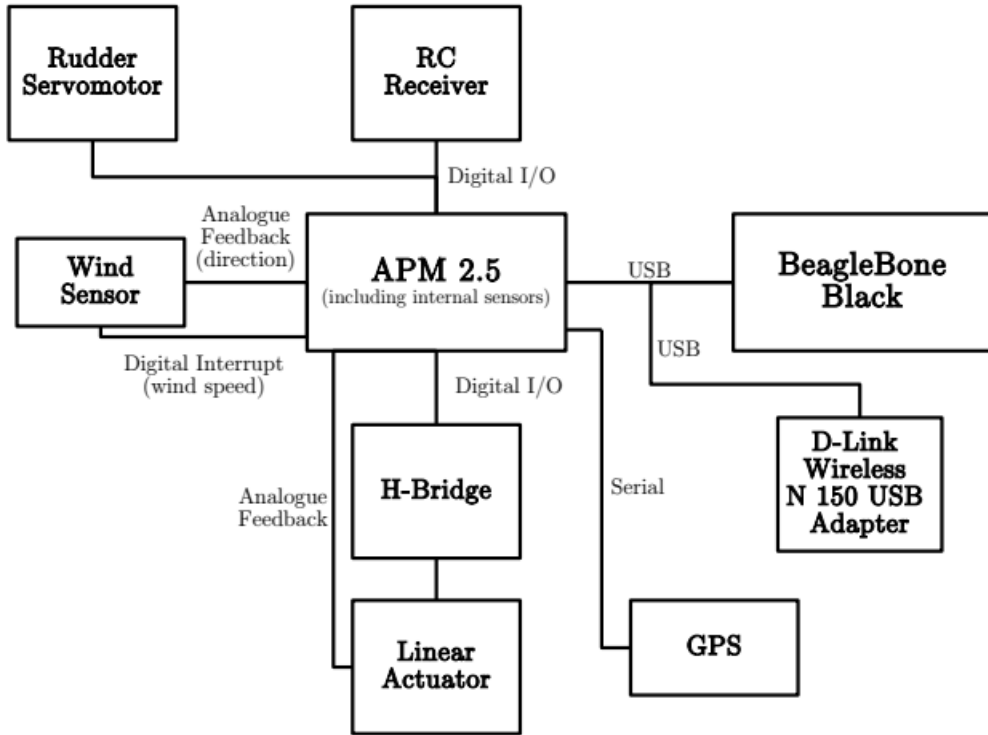


Figure 2.9: Platform developed by UCT sailboat

As illustrated in Figure 2.9 the rudder is controlled with a servomotor and the sail with a linear actuator. It is quite common to make use of either control methods when it comes to controlling the sail or rudder. One problem noted in [1], is the inaccurate data from the wind sensor and this will be taken into account when designing the platform. The next important part of the platform is the base station used for communicating with the sailboat. One such base station GUI developed by [2]. The base station, as previously mentioned, monitors the important states of the sailboat, as the heading angle, rudder and sail command. The base station is also used to send data and commands to the sail boat when required.

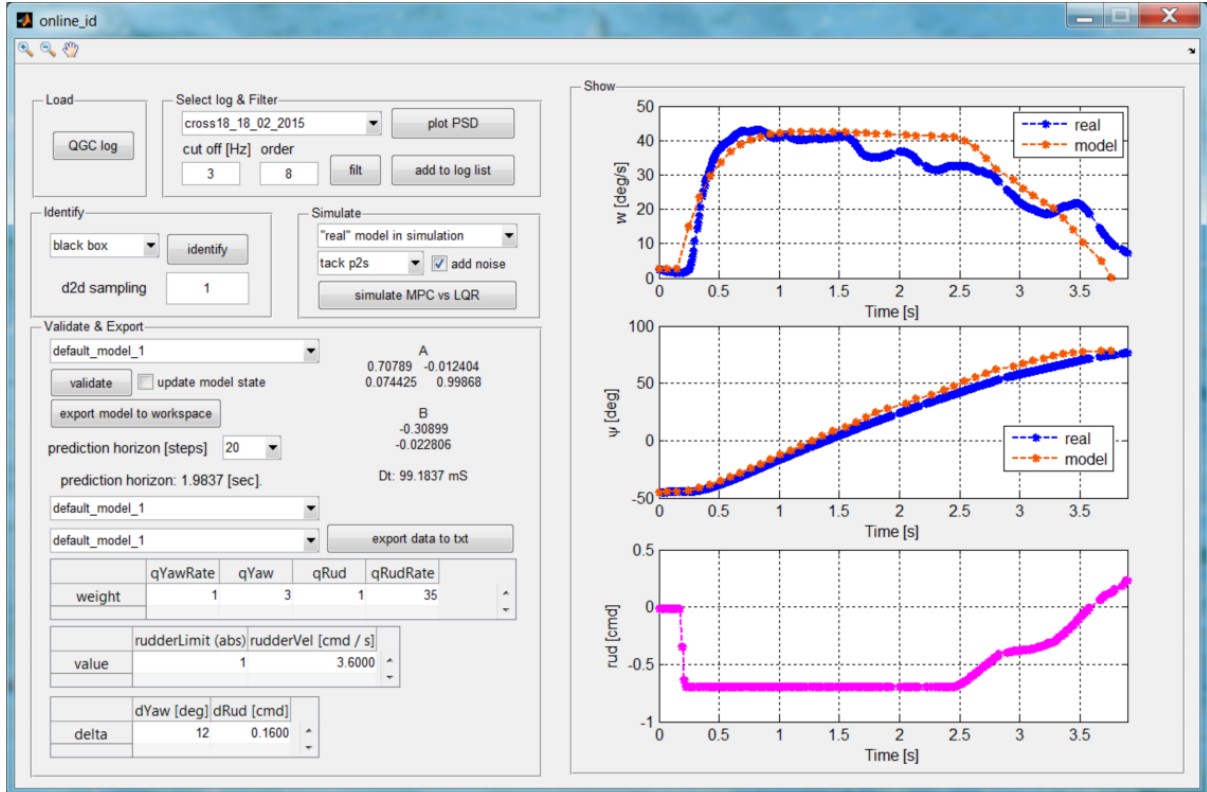


Figure 2.10: GUI developed for sailboat monitoring

2.4. Usages of USV

USV's has enabled data acquisitions that was thought to be unobtainable. Saildrone [6], founded in 2014, a company that specialize in the gathering of ocean data. The USV deployed by Saildrone is illustrated in Figure 2.11. The data that the USV gathers ranges from ocean temperature, humidity, pressure, wind speed and direction.

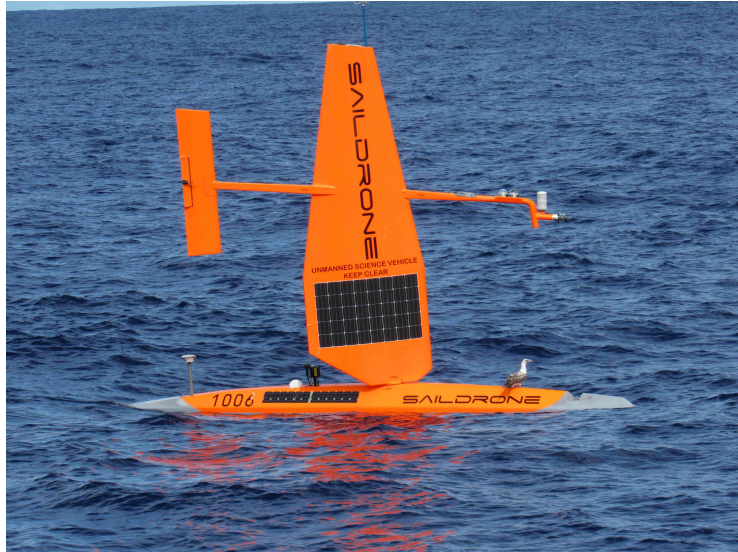


Figure 2.11: Saildrone's USV

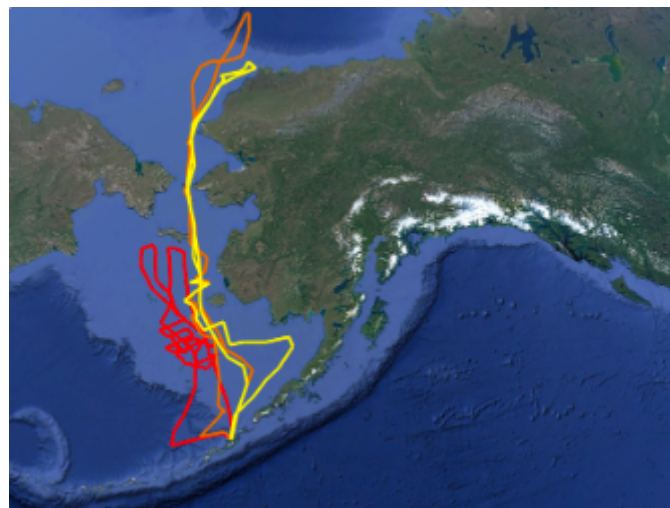


Figure 2.12: Routes of the USV's in Arctic Mission

USV's also allow for exploration of unknown ocean area's, with accompanied sensor USV's can also map out the ocean floor. One of the recent missions completed by Saildrone, was the 2017 Arctic Mission. Saildrone deployed three USV's from the Dutch Harbor in Alaska. Two of the vehicles were equipped with the CO₂ measuring devices and camera's for capturing video and photo footage of northern fur seals. The third vehicle is equipped with an echo sounder for surveying walleye pollock, nothern fur seals and the elusive North Pacific right whale. The three routes of the vehicles are illustrated in Figure 2.12.

Saildrone is one of few companies/organisations that has developed the capable technology to make use of USV. To this extent a lot of research is still needed to develop USV and also is needed to utilise the data in the oceans. This is especially true in undeveloped countries and the ocean's surrounding these countries.

Chapter 3

Modeling of Ocean Vessels

This chapter models a standard ocean vessel in six degrees of freedom. It also introduces the definitions associated with movement in each direction of freedom. The chapter also take into account the forces and moments generated by hydrodynamics and restoration of an ocean vessel. The chapter continues to model the environmental disturbances experience by a semi-submerged ocean vessel. The environmental disturbances are wind, waves and ocean currents.

3.1. Standard Ocean Vessel Notation

An ocean vessels are modelled in six degrees of freedom, requiring six independent coordinates to determine its position and orientation. The first three coordinates corresponding to position (x, y, z) and their first time derivatives, translation motion along the x -, y -, and z -axes. The last three coordinates (ϕ, θ, ψ) and their first time derivatives describing orientation and rotational motion [7]. Figure 3.1 illustrates the motion variables of an ocean vessel with the six independent coordinates.

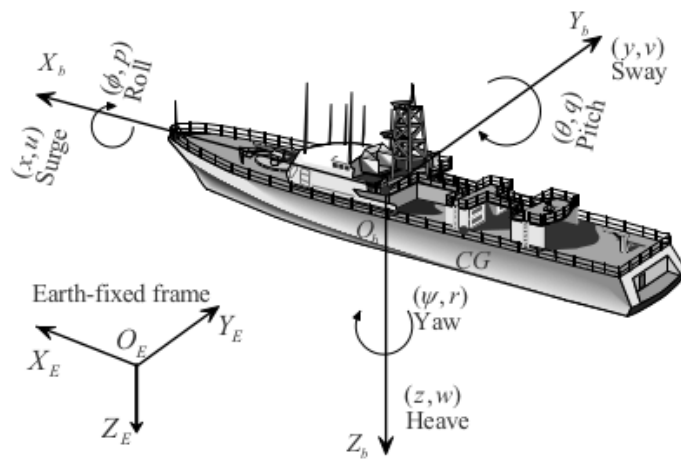


Figure 3.1: Motion variables for an ocean vessel

The SNAME(Society of Naval Architects and Marine Engineers) established the notation for the six different motion components as *surge*, *sway*, *heave*, *roll*, *pitch* and *yaw*. Table A.1 summarizes the SNAME notation for ocean vessels.

Two reference models are used to determine the equations of motion, namely the inertial to earth frame $O_eX_eY_eZ_e$ that may be displaced to overlap with the vessel's fixed coordinates in some initial condition and the body-fixed frame $O_bX_bY_bZ_b$, illustrated in Figure 3.1. The most common used position for the body-fixed frame results in symmetry about the $O_bX_bZ_b$ -plane and approximate symmetry about the $O_bY_bZ_b$. The body axes coincides with the axes of inertia and are usually defines as follows: O_bX_b is the longitudinal axis, O_bY_b is the transverse axis and O_bZ_b is the normal axis. Below are the vectors used to describe the general motion of an ocean vessel:

$$\mathbf{n} = [\mathbf{n}_1 \mathbf{n}_2]^T \quad (3.1)$$

$$\mathbf{v} = [\mathbf{v}_1 \mathbf{v}_2]^T \quad (3.2)$$

$$\boldsymbol{\tau} = [\boldsymbol{\tau}_1 \boldsymbol{\tau}_2]^T \quad (3.3)$$

$$\mathbf{n}_1 = [x \ y \ z]^T \quad (3.4) \qquad \mathbf{n}_2 = [\phi \ \theta \ \psi]^T \quad (3.5)$$

$$\mathbf{v}_1 = [u \ v \ w]^T \quad (3.6) \qquad \mathbf{v}_2 = [p \ q \ r]^T \quad (3.7)$$

$$\boldsymbol{\tau}_1 = [X \ Y \ Z]^T \quad (3.8) \qquad \boldsymbol{\tau}_2 = [K \ M \ N]^T \quad (3.9)$$

where \mathbf{n} denotes the position and orientation vector with coordinates in the earth fixed frame, \mathbf{v} denotes the linear and angular velocity vector with coordinates in the body-fixed frame and $\boldsymbol{\tau}$ denotes the forces and moments acting on the vessel in the body-fixed frame. The vessel dynamics are divided into two parts known as *kinematics* and *kinetics*.

3.2. Kinematics

Kinematics looks at the motion of the vessel without directly considering the forces affecting the motion. The first time derivative of the position vectors \mathbf{n}_1 and \mathbf{n}_2 is related to the linear velocity vector \mathbf{v}_1 and \mathbf{v}_2 via the following transformations,

$$\dot{\mathbf{n}}_1 = \mathbf{J}_1(\mathbf{n}_2)\mathbf{v}_1 \quad (3.10)$$

$$\dot{\mathbf{n}}_2 = \mathbf{J}_2(\mathbf{n}_2)\mathbf{v}_2 \quad (3.11)$$

where $\mathbf{J}_1(\mathbf{n}_2)$ and $\mathbf{J}_2(\mathbf{n}_2)$ are transformation matrices, which is related through the functions of the Euler angles: roll(ϕ), pitch(θ) and yaw(ψ). The \mathbf{J}_1 transformation matrix is given by

$$\mathbf{J}_1(\mathbf{n}_2) = \begin{bmatrix} \cos(\psi)\cos(\theta) & -\sin(\psi)\cos(\theta) + \sin(\phi)\sin(\theta)\cos(\psi) & \sin(\psi)\sin(\phi) + \sin(\theta)\cos(\psi)\cos(\phi) \\ \sin(\psi)\cos(\theta) & \cos(\psi)\cos(\phi) + \sin(\phi)\sin(\theta)\sin(\psi) & -\cos(\psi)\sin(\phi) + \sin(\theta)\sin(\psi)\cos(\phi) \\ -\sin(\theta) & \sin(\phi)\cos(\theta) & \cos(\phi)\cos(\theta) \end{bmatrix} \quad (3.12)$$

and the transformation matrix \mathbf{J}_2 is given by,

$$\mathbf{J}_2(\mathbf{n}_2) = \begin{bmatrix} 1 & -\sin(\phi)\tan(\theta) & \cos(\phi)\tan(\theta) \\ 0 & \cos(\phi) & -\sin(\phi) \\ 0 & \sin(\phi)/\cos(\theta) & \cos(\phi)/\cos(\theta) \end{bmatrix} \quad (3.13)$$

When $\theta = \pi/2$, the transformation matrix $\mathbf{J}_2(\mathbf{n}_2)$ becomes singular, however this is unlikely to happen when practically testing an ocean vessel, because of the metacentric restoring forces. Combining Equation 3.12 and Equation 3.13 results in the kinematics of an ocean vessel.

$$\begin{bmatrix} \dot{\mathbf{n}}_1 \\ \dot{\mathbf{n}}_2 \end{bmatrix} = \begin{bmatrix} \mathbf{J}_1(\mathbf{n}_2) & 0_{3 \times 3} \\ 0_{3 \times 3} & \mathbf{J}_2(\mathbf{n}_2) \end{bmatrix} \begin{bmatrix} \mathbf{v}_1 \\ \mathbf{v}_2 \end{bmatrix} = \dot{\mathbf{n}} = \mathbf{J}(\mathbf{n})\mathbf{v} \quad (3.14)$$

3.3. Kinetics

The Newton-Euler formulation [8] defines the balancing forces and moments for a rigid body with a mass of m as follows,

$$\mathbf{f}_{Ob} = \mathbf{m}[\dot{\mathbf{v}}_{Ob}^E + \dot{\mathbf{w}}_{Ob}^E \times \mathbf{r}_{Ob} + \mathbf{w}_{Ob}^E \times \mathbf{v}_{Ob} + \mathbf{w}_{Ob}^E \times (\mathbf{w}_{Ob}^E \times \mathbf{r}_{Ob})] \quad (3.15)$$

$$\mathbf{m}_{Ob} = \mathbf{I}_o \mathbf{w}_{Ob}^E + \dot{\mathbf{w}}_{Ob}^E \times \mathbf{I}_o \mathbf{w}_{Ob}^E + m \mathbf{r}_{Ob} \times (\dot{\mathbf{v}}_{Ob} + \mathbf{w}_{Ob}^E \times \mathbf{v}_{Ob}) \quad (3.16)$$

where \mathbf{f}_{Ob} is the balancing forces, \mathbf{m}_{Ob} the balancing moments and \mathbf{I}_o is the inertia matrix about O_b defined as,

$$\mathbf{I}_o = \begin{bmatrix} I_x & -I_{xy} & -I_{xz} \\ -I_{yx} & I_y & -I_{yz} \\ -I_{zx} & -I_{zy} & I_z \end{bmatrix} \quad (3.17)$$

I_x, I_y and I_z are the moments of inertia about the O_bX_b , O_bY_b and O_bZ_b axes. $I_{xy} = I_{yx}$, $I_{xz} = I_{zx}$ and $I_{yz} = I_{zy}$ are the products of inertia. These quantities are defined as

$$I_x = \int_V (y^2 + z^2) \rho_m dV \quad (3.18)$$

$$I_{xy} = \int_V xy \rho_m dV \quad (3.19)$$

$$I_y = \int_V (x^2 + z^2) \rho_m dV \quad (3.20)$$

$$I_{xz} = \int_V xz \rho_m dV \quad (3.21)$$

$$I_z = \int_V (z^2 + y^2) \rho_m dV \quad (3.22)$$

$$I_{zy} = \int_V zy \rho_m dV \quad (3.23)$$

where ρ_m are the mass density and V the volume of the rigid body. By substituting the definitions defined in Table A.2 into Equations 3.15 and 3.16, results in the equation below,

$$\mathbf{M}_{RB}\dot{\mathbf{v}} + \mathbf{C}_{RB}(\mathbf{v})\mathbf{v} = \tau_{RB} \quad (3.24)$$

where $\mathbf{v} = [u \ v \ w \ p \ q \ r]^T$ is the generalized velocity vector decomposed in the body-fixed frame and $\tau_{\mathbf{RB}} = [X \ Y \ Z \ K \ M \ N]^T$ is the generalized vector of external forces and moments. The rigid body system inertia matrix $\mathbf{M}_{\mathbf{RB}}$ and the rigid body Coriolis and centripetal matrix $\mathbf{C}_{\mathbf{RB}}$ is defined in Equation A.1 and A.2. The generalized external force and moment vector, $\tau_{\mathbf{RB}}$, is a sum of the hydrodynamic force and moment vector $\tau_{\mathbf{H}}$, external disturbance force and moment vector $\tau_{\mathbf{E}}$ and propulsion force and moment vector τ .

3.4. Hydrodynamic Forces and Moments

Hydrodynamic forces and moments can be defined as the forces and moments on a ocean body when the body is forced to oscillate with the wave excitation and no wave are incident on the body. As shown in [9], the hydrodynamic forces and moments acting on a rigid body can be assumed to be linearly superimposed. The forces and moments can be subdivided into three components,

1. Added mass due to the inertia of the surrounding fluid
2. Radiation-induced potential damping due to the energy carried away by the generated surface waves
3. Restoring forces due to Archimedian forces

The hydrodynamic forces and moments vector $\tau_{\mathbf{H}}$ is expressed in the equation below,

$$\tau_{\mathbf{H}} = -\mathbf{M}_{\mathbf{A}}\dot{\mathbf{v}} - \mathbf{C}_{\mathbf{A}}(\mathbf{v})\mathbf{v} - \mathbf{D}(\mathbf{v})\mathbf{v} - \mathbf{g}(\mathbf{n}) \quad (3.25)$$

where $\mathbf{M}_{\mathbf{A}}$ is the added mass matrix, $\mathbf{C}_{\mathbf{A}}(\mathbf{v})$ is the hydrodynamic Coriolis and centripetal matrix, $\mathbf{D}(\mathbf{v})$ is the damping matrix and $\mathbf{g}(\mathbf{n})$ is the position and orientation depending vector of restoring forces and moments. The added mass $\mathbf{M}_{\mathbf{A}}$ is given below,

$$\mathbf{M}_{\mathbf{A}} = \begin{bmatrix} X_{\dot{u}} & X_{\dot{v}} & X_{\dot{w}} & X_{\dot{p}} & X_{\dot{q}} & X_{\dot{r}} \\ Y_{\dot{u}} & Y_{\dot{v}} & Y_{\dot{w}} & Y_{\dot{p}} & Y_{\dot{q}} & Y_{\dot{r}} \\ Z_{\dot{u}} & Z_{\dot{v}} & Z_{\dot{w}} & Z_{\dot{p}} & Z_{\dot{q}} & Z_{\dot{r}} \\ K_{\dot{u}} & K_{\dot{v}} & K_{\dot{w}} & K_{\dot{p}} & K_{\dot{q}} & K_{\dot{r}} \\ M_{\dot{u}} & M_{\dot{v}} & M_{\dot{w}} & M_{\dot{p}} & M_{\dot{q}} & M_{\dot{r}} \\ N_{\dot{u}} & N_{\dot{v}} & N_{\dot{w}} & N_{\dot{p}} & N_{\dot{q}} & N_{\dot{r}} \end{bmatrix} \quad (3.26)$$

The hydrodynamic Coriolis and centripetal matrix is given below,

$$\mathbf{C}_{\mathbf{A}}(\mathbf{v}) = \begin{bmatrix} 0 & 0 & 0 & 0 & -a_3 & a_2 \\ 0 & 0 & 0 & a_3 & 0 & -a_1 \\ 0 & 0 & 0 & -a_2 & a_1 & 0 \\ 0 & -a_3 & a_2 & 0 & -b_3 & b_2 \\ a_3 & 0 & -a_1 & b_3 & 0 & -b_1 \\ -a_2 & a_1 & 0 & -b_2 & b_1 & 0 \end{bmatrix} \quad (3.27)$$

where a_1 , a_2 , a_3 , b_1 , b_2 and b_3 are defined in Equations A.3, A.4, A.5, A.6, A.7 and A.8.

The general hydrodynamic damping experienced by ocean vessels is the potential damping, skin friction, wave drift damping and damping due to vortex shedding. The hydrodynamic damping can be expressed in a general form as below,

$$\mathbf{D}(\mathbf{v}) = \mathbf{D} + \mathbf{D}_n(\mathbf{v}) \quad (3.28)$$

where the linear damping matrix \mathbf{D} is given below,

$$\mathbf{D} = - \begin{bmatrix} X_u & X_v & X_w & X_p & X_q & X_r \\ Y_u & Y_v & Y_w & Y_p & Y_q & Y_r \\ Z_u & Z_v & Z_w & Z_p & Z_q & Z_r \\ K_u & K_v & K_w & K_p & K_q & K_r \\ M_u & M_v & M_w & M_p & M_q & M_r \\ N_u & N_v & N_w & N_p & N_q & N_r \end{bmatrix} \quad (3.29)$$

3.5. Restoring Forces and Moments

Static stability considerations due to restoring forces are usually referred to as *metacentric stability* in the hydrostatic literature. A metacentric stable vessel will resist inclinations away from its steady-state or equilibrium points in heave, roll and pitch. For surface vehicles, the restoring force will depend on the vessel's metacentric height, the location of CG and CB , as well as the shape and size of the water plane. Let A_{wp} denote the water plane area and

$$GM_T = \text{transverse metacentric height}(m) \quad (3.30)$$

$$GM_T = \text{longitudinal metacentric height}(m) \quad (3.31)$$

The metacentric height GM_i , where $i \in T, L$, is the distance between the metacentre M_i and the CG , as shown in Figure 3.2.

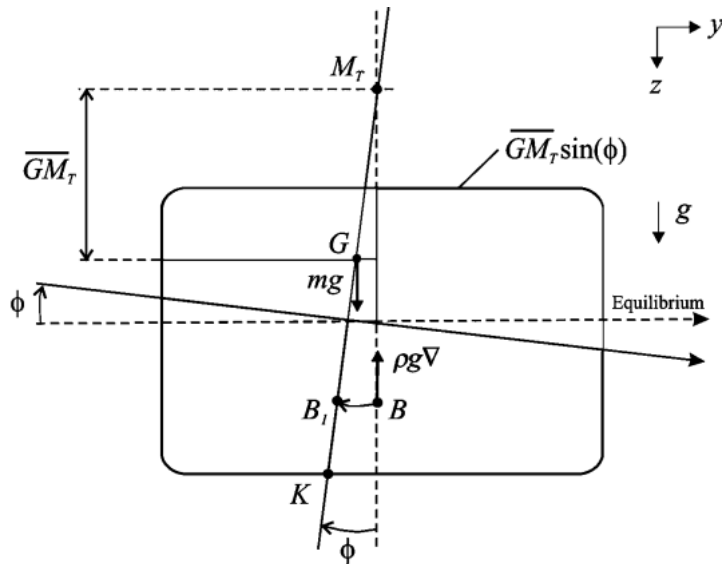


Figure 3.2: Transverse metacentric stability

For a floating vessel at rest, Archimedes stated that buoyancy and weight are in balance.

$$mg = \rho g \nabla \quad (3.32)$$

where m is the mass of the vessel, g gravitational force, ρ density of water and ∇ the nominal displaced water volume. Hence, the hydrostatic force in heave will be the difference between the gravitational and the buoyancy forces:

$$Z = mg - \rho g [\nabla + \delta \nabla(z)] = -\rho g \delta \nabla(z) \quad (3.33)$$

where the change in displaced water $\delta \nabla(z)$ is due to variations in heave position z . This can be written as

$$\delta \nabla(z) = \int_0^z A_{\omega\rho}(\delta) d\delta \quad (3.34)$$

where $A_{\omega\rho}(\delta)$ is the water plane area of the vessel as a function of the heave position. For conventional rigs and ships, however, it is common to assume that $A_{\omega\rho}(\delta) \approx A_{\omega\rho}(0)$ is constant for small perturbations in z . Hence, the restoring force Z will be linear in z , that is

$$Z \approx -\rho g A_{\omega\rho}(0) z \quad (3.35)$$

Recall that if a floating vessel is forced downwards by an external force such that $z \geq 0$, the buoyancy force becomes larger than the constant gravitational force since the submerged volume ∇ increases by $\delta \nabla$ to $\nabla + \delta \nabla$. This is physically equivalent to a spring with stiffness $Z_z = -\rho g A_{\omega\rho}(0)$ and position z . The restoring force expressed in body frame δf_r^b can therefore be written as

$$\delta f_r^b = -\rho g \begin{bmatrix} -\sin(\theta) \\ \cos(\theta)\sin(\phi) \\ \cos(\theta)\cos(\phi) \end{bmatrix} \int_0^z A_{\omega\rho}(\delta) d\delta \quad (3.36)$$

From Figure 3.2 it is seen that the moment arms in roll and pitch can be related to the moment arms $GM_T \sin(\phi)$ and $GM_L \sin(\theta)$ in roll and pitch and a z -direction force pair with magnitude $W = B = \rho g \nabla$. Therefore,

$$r_r^b = \begin{bmatrix} -GM_L \sin(\theta) \\ GM_T \sin(\phi) \\ 0 \end{bmatrix} \quad (3.37)$$

$$f_r^b = -0 \rho g \nabla \begin{bmatrix} -\sin(\theta) \\ \cos(\theta)\sin(\phi) \\ \cos(\theta)\cos(\phi) \end{bmatrix} \quad (3.38)$$

By neglecting the moment contribution due to δf_r^b , consider only f_r^b , implies that the restoring moment becomes

$$m_r^b = r_r^b \times f_r^b = -\rho g \nabla \begin{bmatrix} GM_T \sin(\phi) \cos(\theta) \cos(\phi) \\ GM_L \sin(\theta) \cos(\theta) \cos(\phi) \\ (GM_T - GM_L \cos(\theta)) \sin(\phi) \sin(\theta) \end{bmatrix} \quad (3.39)$$

The assumption that $r_r^b \times \delta f_r^b = 0$ (no moments due to heave) is a good assumption since this term is small compared to $r_r^b \times f_r^b$. The restoring forces and moments are finally written as

$$\mathbf{g}(\mathbf{n}) = - \begin{bmatrix} \delta \mathbf{f}_r^b \\ \mathbf{m}_r^b \end{bmatrix} \quad (3.40)$$

$$\mathbf{g}(\mathbf{n}) = \begin{bmatrix} \rho g \int_0^z A_{\omega\rho}(\delta) d\delta \sin(\theta) \\ \rho g \int_0^z A_{\omega\rho}(\delta) d\delta \cos(\theta) \sin(\phi) \\ \rho g \int_0^z A_{\omega\rho}(\delta) d\delta \cos(\theta) \cos(\phi) \\ \rho g \nabla G M_T \sin(\phi) \cos(\theta) \cos(\phi) \\ \rho g \nabla G M_L \sin(\theta) \cos(\theta) \cos(\phi) \\ \rho g \nabla (G M_T + -G M_L \cos(\theta)) \sin(\phi) \sin(\theta) \end{bmatrix} \quad (3.41)$$

3.6. Environmental Disturbances

The forces and moments induced by the environmental disturbances is defined by the vector τ_E and includes ocean currents, waves(wind generated) and wind.

$$\tau_E = \tau_E^{cu} + \tau_E^{wa} + \tau_E^{wi} \quad (3.42)$$

where τ_E^{cu} , τ_E^{wa} and τ_E^{wi} are vectors of forces and moments induced by ocean currents, waves and wind.

3.6.1. Current-induced Forces and Moments

The current induced forces and moments vector τ_E^{cu} is given by

$$\tau_E^{cu} = (\mathbf{M}_{RB} + \mathbf{M}_A)\dot{\mathbf{v}}_c + \mathbf{C}(\mathbf{v}_r)\mathbf{v}_r - \mathbf{C}(\mathbf{v})\mathbf{v} + \mathbf{D}(\mathbf{v}_r)\mathbf{v}_r - \mathbf{D}(\mathbf{v})\mathbf{v} \quad (3.43)$$

where $\mathbf{v}_r = \mathbf{v} - \mathbf{v}_c$ and $\mathbf{v}_c = [u_c, v_c, w_c, 0, 0, 0]^T$ is a vector irrotational body-fixed current velocities. Take the earth-fixed velocity vector denoted by $[u_c^E, v_c^E, w_c^E]^T$, then the bodyfixed components $[u_c, v_c, w_c]^T$ can be calculated by

$$\begin{bmatrix} u_c \\ v_c \\ w_c \end{bmatrix} = \mathbf{J}_1^T(\mathbf{n}_2) \begin{bmatrix} u_C^E \\ v_C^E \\ w_C^E \end{bmatrix} \quad (3.44)$$

3.6.2. Wave-induced Forces and Moments

The vector τ_E^{wa} of the wave-induced forces and moments is given by

$$\tau_E^{wa} = \begin{bmatrix} \sum_{i=1}^N \rho g B L T \cos(\beta) s_i(t) \\ \sum_{i=1}^N \rho g B L T \sin(\beta) s_i(t) \\ 0 \\ 0 \\ 0 \\ \sum_{i=1}^N \frac{1}{24} \rho g B L (L^2 - B^2) \sin(2\beta) s_i^2(t) \end{bmatrix} \quad (3.45)$$

where β is the vessel's heading(encounter) angle, illustrated in Figure , ρ is the water density, L is the length of the vessel, B is the breadth of the vessel and T is the draft of the vessel. Ignoring the higher-order terms of the wave amplitude, the wave slope $s_i(t)$ for the wave component i is defined by

$$s_i(t) = A_i \frac{2\pi}{\lambda_i} \sin(\omega_{ei} t + \phi_i) \quad (3.46)$$

where A_i is the wave amplitude, λ_i is the wave length, ω_{ei} is the encounter frequency and ϕ_i is a random phase uniformly distributed and constant with time $[0 \ 2\pi)$ corresponding to the wave component i .

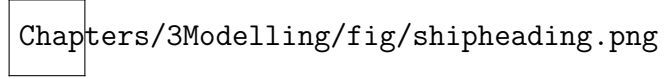


Figure 3.3: Ocean vessel's heading angle

3.6.3. Wind-induced Forces and Moments

When the ocean vessel is at rest the vector $\tau_E^{\omega i}$ of the wind induced forces and moments is given by

$$\tau_E^{\omega i} = \begin{bmatrix} C_X(\gamma_\omega)A_{F\omega} \\ C_Y(\gamma_\omega)A_{L\omega} \\ C_Z(\gamma_\omega)A_{F\omega} \\ C_K(\gamma_\omega)A_{L\omega}H_{L\omega} \\ C_M(\gamma_\omega)A_{F\omega}H_{F\omega} \\ C_N(\gamma_\omega)A_{L\omega}L_{oa} \end{bmatrix} \quad (3.47)$$

where V_ω is the wind speed, ρ_a is the air density, $A_{F\omega}$ is the frontal projected area, $A_{L\omega}$ is the lateral projected area, $H_{F\omega}$ is the centroid of $A_{F\omega}$ above the water line, $H_{L\omega}$ is the centroid of $A_{L\omega}$ above the water line, L_{oa} is the over all length of the vessel, γ_ω is the angle of relative wind of the vessel bow, illustrated in Figure 3.4 and is given by

$$\gamma_\omega = \psi - \beta_\omega - \pi \quad (3.48)$$

where β_ω being the wind direction. All the wind coefficients(look-up tables) $C_X(\gamma_\omega)A_{F\omega}$, $C_Y(\gamma_\omega)A_{L\omega}$, $C_Z(\gamma_\omega)A_{F\omega}$, $C_K(\gamma_\omega)A_{L\omega}H_{L\omega}$, $C_M(\gamma_\omega)A_{F\omega}H_{F\omega}$ and $C_N(\gamma_\omega)A_{L\omega}L_{oa}$ are computed numerically or by experiments in a wind tunnel as shown in [10].

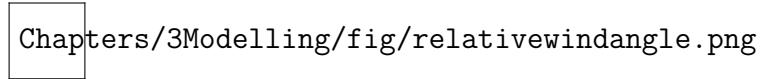


Figure 3.4: Wind angle on vessel

When the vessel is moving the vector $\tau_E^{\omega i}$ is given by

$$\tau_E^{\omega i} = \begin{bmatrix} C_X(\gamma_{r\omega})A_{F\omega} \\ C_Y(\gamma_{r\omega})A_{L\omega} \\ C_Z(\gamma_{r\omega})A_{F\omega} \\ C_K(\gamma_{r\omega})A_{L\omega}H_{L\omega} \\ C_M(\gamma_{r\omega})A_{F\omega}H_{F\omega} \\ C_N(\gamma_{r\omega})A_{L\omega}L_{oa} \end{bmatrix} \quad (3.49)$$

where

$$V_{r\omega} = \sqrt{u_{r\omega}^2 + v_{r\omega}^2} \quad (3.50)$$

$$\gamma_{r\omega} = -\arctan2(v_{r\omega}, u_{r\omega}) \quad (3.51)$$

with

$$u_{r\omega} = u - V_\omega \cos(\beta_\omega - \psi) \quad (3.52)$$

$$v_{r\omega} = v - V_\omega \cos(\beta_\omega - \psi) \quad (3.53)$$

3.7. Simplifications of 6-DOF

3.7.1. Standard 3-DOF Horizontal Model

The horizontal motion of a surface ship in a horizontal plane is often described by the motion component in surge, sway and yaw. You choose $\mathbf{n} = [x, y, \psi]^T$ and $\mathbf{v} = [u, v, r]^T$. Figure 3.5 illustrates the motion variables in this case.

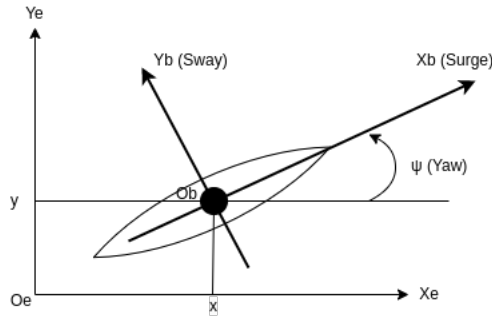


Figure 3.5: Standard 3-DOF Horizontal Model

Assumptions

1. The motion in roll, pitch and heave is ignored. This means that we ignore the dynamics associated with the motion in heave, roll and pitch, i.e., $z = 0$, $w = 0$, $\phi = 0$, $\theta = 0$ and $q = 0$.
2. The vessel has homogeneous mass distribution and xz -plane of symmetry so that

$$I_{xy} = I_{yz} = 0 \quad (3.54)$$

3. The center of gravity and center of buoyancy are located vertically on the z-axis

The vessel dynamics in a horizontal plane is simplified as follows:

$$\dot{\mathbf{n}} = \mathbf{J}(\mathbf{n})\mathbf{v} \quad (3.55)$$

$$\mathbf{M}\dot{\mathbf{v}} = -\mathbf{C}(\mathbf{v})\mathbf{v} - (\mathbf{D} + \mathbf{D}_n(\mathbf{v}))\mathbf{v} + \mathbf{f}_E \quad (3.56)$$

where the matrices $\mathbf{J}(\mathbf{n})$, \mathbf{M} , \mathbf{D} and $\mathbf{D}_n(\mathbf{v})$ are given by

$$J(n) = \begin{bmatrix} \cos(\psi) & -\sin(\psi) & 0 \\ \sin(\psi) & \cos(\psi) & 0 \\ 0 & 0 & 1 \end{bmatrix} \quad (3.57)$$

$$M = \begin{bmatrix} m - X_{\dot{u}} & 0 & 0 \\ 0 & m - Y_{\dot{v}} & mx_g - Y_r \\ 0 & mx_g - Y_{\dot{r}} & I_z - N_{\dot{r}} \end{bmatrix} \quad (3.58)$$

$$C(v) = \begin{bmatrix} 0 & 0 & -m(x_g r + v) + Y_{\dot{v}v - Y_{\dot{r}r}} \\ 0 & 0 & mu - X_{\dot{u}u} \\ m(x_g r + v) - Y_{\dot{v}v - Y_{\dot{r}r}} & -mu + X_{\dot{u}u} & 0 \end{bmatrix} \quad (3.59)$$

$$D = \begin{bmatrix} X_u & 0 & 0 \\ 0 & Y_v & Y_r \\ 0 & N_v & N_r \end{bmatrix} \quad (3.60)$$

$$D_n(v) = \begin{bmatrix} X_{|u|u}|u| & 0 & 0 \\ 0 & Y_{|v|v}|v| + Y_{|r|v}|r| & Y_{|v|r}|v| \\ 0 & N_{|v|v}|v| + N_{|r|v}|r| & N_{|v|r}|v| + X_{|r|r}|r| \end{bmatrix} \quad (3.61)$$

The propulsion force and moment vector τ is given by

$$\tau = \begin{bmatrix} \tau_u \\ 0 \\ \tau_r \end{bmatrix} \quad (3.62)$$

The above propulsion force and moment vector τ implies that we are considering a surface vessel, which does not have an independent actuator in the sway. The environmental disturbance vector τ_E is given by

$$\tau = \begin{bmatrix} \tau_{uE} \\ \tau_{vE} \\ \tau_{rE} \end{bmatrix} \quad (3.63)$$

3.7.2. Simplified 3-DOF Horizontal Model

In some cases we can ignore the off-diagonal terms of the matrices \mathbf{M} and \mathbf{D} , all elements of the nonlinear damping matrix $\mathbf{D}_n(\mathbf{v})$. These assumptions hold when the vessel has three planes of symmetry, for which the axes of the body-fixed reference frame are chosen to be parallel to the principle axis of the displaced fluid, which are equal to the principle axis of the vessel. Most ships have port/starboard symmetry and moreover, bottom/top symmetry is not required fore horizontal motion. Ship fore/aft nonsymmetry implies that the off-diagonal terms of the inertia and damping matrices are nonzero. However, these terms are small compared to the main diagonal terms. Furthermore, disturbances induced by the waves, wind and ocean currents are ignored. The dynamics of the vessel in the horizontal plane is simplified as follows:

$$\dot{\mathbf{n}} = \mathbf{J}(\mathbf{n})\mathbf{v} \quad (3.64)$$

$$\mathbf{M}\dot{\mathbf{v}} = -\mathbf{C}(\mathbf{v})\mathbf{v} - \mathbf{D}\mathbf{v} + \tau \quad (3.65)$$

where the matrices $\mathbf{J}(\mathbf{n})$, \mathbf{M} , $\mathbf{C}(\mathbf{v})$ and \mathbf{D} are given by

$$\mathbf{J}(n) = \begin{bmatrix} \cos(\psi) & -\sin(\psi) & 0 \\ \sin(\psi) & \cos(\psi) & 0 \\ 0 & 0 & 1 \end{bmatrix} \quad (3.66)$$

$$\mathbf{M} = \begin{bmatrix} m_{xy} & 0 & 0 \\ 0 & m_{xy} & 0 \\ 0 & 0 & m_{33} \end{bmatrix} \quad (3.67)$$

$$\mathbf{C}(v) = \begin{bmatrix} 0 & 0 & -m_{xy}v \\ 0 & 0 & m_{xy}u \\ m_{xy}v & -m_{xy}u & 0 \end{bmatrix} \quad (3.68)$$

$$\mathbf{D} = \begin{bmatrix} d_{xy} & 0 & 0 \\ 0 & d_{xy} & 0 \\ 0 & 0 & d_{33} \end{bmatrix} \quad (3.69)$$

with

$$m_{xy} = m - X_{\dot{u}} = m - Y_{\dot{v}} \quad (3.70)$$

$$m_{33} = I_z - N_{\dot{r}} \quad (3.71)$$

$$d_{xy} = -X_u = -Y_v \quad (3.72)$$

$$d_{33} = -N_r \quad (3.73)$$

3.8. Summary

The combined six degrees of freedom equations of motion is shown below:

$$\dot{\mathbf{n}} = \mathbf{J}(n)\mathbf{v} \quad (3.74)$$

$$M\dot{\mathbf{v}} = -\mathbf{C}(v)\mathbf{v} - \mathbf{D}(v)\mathbf{v} - \mathbf{g}(n) + \boldsymbol{\tau} + \boldsymbol{\tau}_E \quad (3.75)$$

where

$$\mathbf{M} = \mathbf{M}_{RB} + \mathbf{M}_A \quad (3.76)$$

$$\mathbf{C}(v) = \mathbf{C}_{RB}(v) + \mathbf{C}_A(v) \quad (3.77)$$

$\mathbf{J}(\mathbf{n})$, equation 3.12 and 3.13, is the transformation matrix which translate \mathbf{v}_1 and \mathbf{v}_2 through the functions of the Euler angles to $\dot{\mathbf{n}}_1$ and $\dot{\mathbf{n}}_2$. $\mathbf{C}(\mathbf{v})$ is the linear combination of the rigid body Coriolis and centripetal matrix $\mathbf{C}_{RB}(\mathbf{v})$, equation A.2 and the hydrodynamic Coriolis and centripetal matrix $\mathbf{C}_A(\mathbf{v})$, equation 3.27. $\mathbf{D}(\mathbf{v})$, equation 3.29, is the hydrodynamic damping and $\mathbf{g}(\mathbf{n})$, equation 3.28, is the restoring forces and moments, equation ???. The propulsion forces and moments is modelled by $\boldsymbol{\tau}$ and the environmental disturbances by $\boldsymbol{\tau}_E$.

3.9. Simulation Results

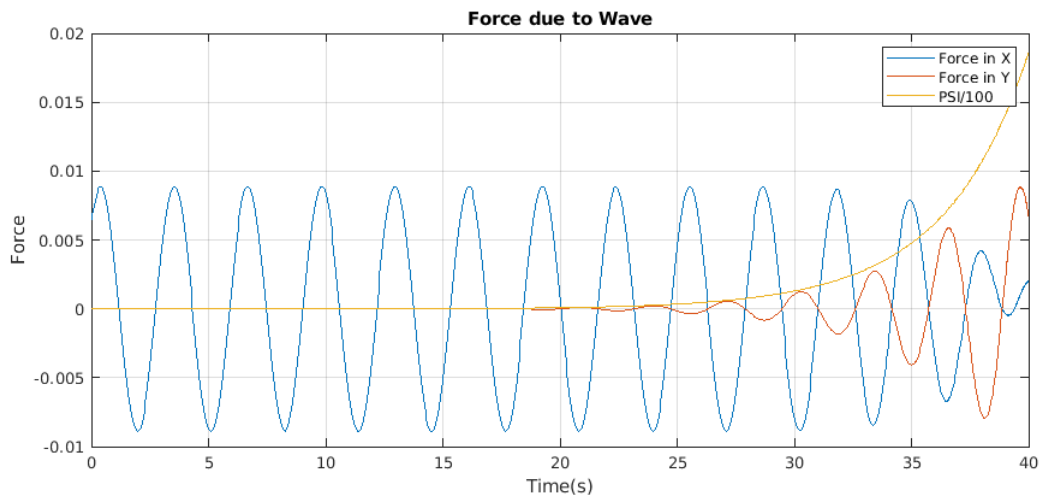


Figure 3.6: Forces caused by waves in x- and y-direction

Chapter 4

Modeling of a Fixed-Wing Sail, Keel and Rudder

This chapter the modeling of a fixed-wing sail is considered. Traditional sails consist of a mainsail and a jib [11]. The sail considered in the chapter is a fixed-wing sail that is fully autonomous. The sail takes inspiration from a free rotating fixed wing sail [12] and fixed-wing sail [1]. The chapter models the forces experienced by adding a fixed-wing sail to the model described in Chapter 3. Also discussed in this chapter is the modelling of forces, moments and constraints caused by a rudder and keel.

4.1. Rudder Theory

4.1.1. Rudder Theory and Terminology

The rudder of a ocean vessel is located at the rear of the vessel and is used for steering. The rudder is usually completely submerged and therefor the forces applicable to the rudder is only hydrodynamic. A rudder changes steers a ocean vessel by generating a lifting force that causes the vessel change its heading [13]. The rudder is fundamental to the safe operation of the ocean vessel. In the case of a sailboat a rudder is very important in establishing an angle of attack and adjusting the sail direction accordingly. The terminology associated with a lifting foil is shown below, where a rudder only differs with having no maximum camber, because it is symmetrical.

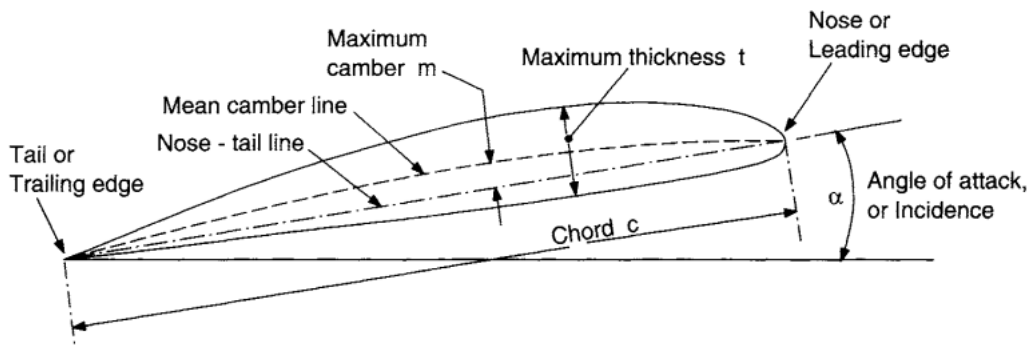


Figure 4.1: Terminology of a lifting foil

4.1.2. Hydrodynamics of a Rudder

The lifting action of the rudder arises from the difference in the average pressure of the fluid over the upper and lower surfaces of the rudder, illustrated in Figure 4.2.

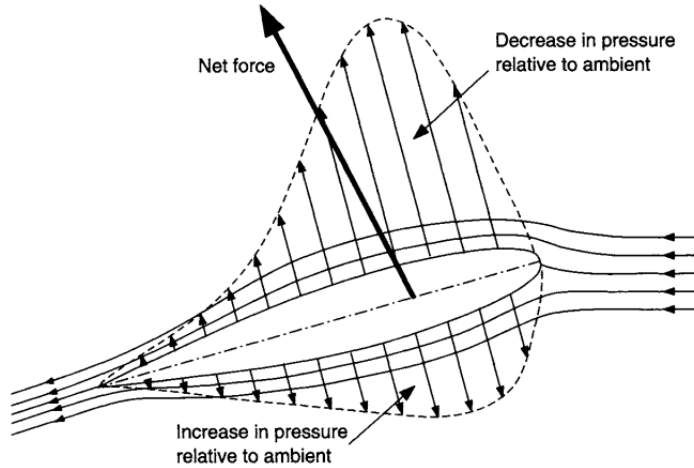


Figure 4.2: Pressure around the rudder

The total force on the rudder consists of a *lift* component perpendicular to the fluid stream U_0 and a *drag* component parallel to U_0 , illustrated in Figure 4.3.

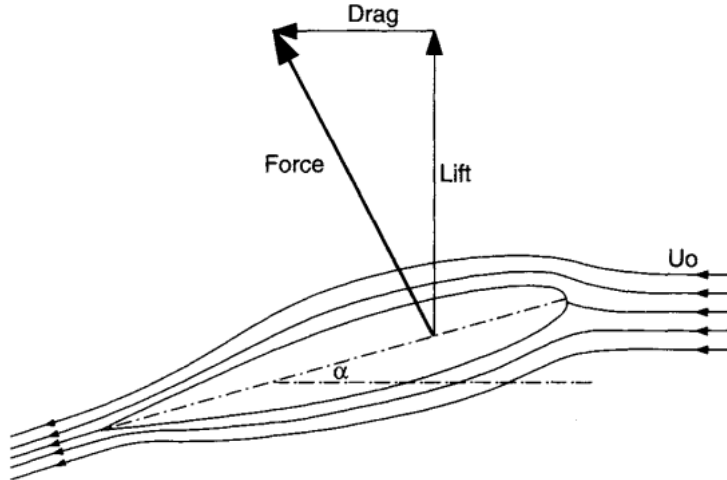


Figure 4.3: Lift and drag force on rudder

These components are usually presented in terms of dimensionless coefficients for a given rudder angle of attack α , where α is the angle between the rudder and the direction of flow.

$$C_L = \frac{Lift}{0.5\rho AU_0^2} \quad (4.1)$$

$$C_D = \frac{Drag}{0.5\rho AU_0^2} \quad (4.2)$$

where A is the rudder area, U_0 the fluid free-stream speed and ρ the fluid density. C_L and C_D depend on the rudder geometry, the incidence to the incoming fluid flow and the Reynolds number(Re).

4.1.3. Rudder Forces and Moments

The forces and moments experienced by a sailboat due to the rudder are defined in [14]. The equations formulated for the forces and moments are illustrated below

$$X_{rud} = C_{X\delta_R} \sin(\alpha_R) \sin(\delta_R) \times \frac{1}{2} \rho_w v_B^2 L_{WL} D_K \quad (4.3)$$

$$Y_{rud} = C_{Y\delta_R} \sin(\alpha_R) \cos(\delta_R) \cos(\phi) \times \frac{1}{2} \rho_w v_B^2 L_{WL} D_K \quad (4.4)$$

$$K_{rud} = C_{K\delta_R} \sin(\alpha_R) \sin(\delta_R) \times \frac{1}{2} \rho_w v_B^2 L_{WL} D_K \quad (4.5)$$

$$N_{rud} = C_{N\delta_R} \sin(\alpha_R) \cos(\delta_R) \cos(\phi) \times \frac{1}{2} \rho_w v_B^2 L_{WL} D_K \quad (4.6)$$

where $C_{X\delta_R}$, $C_{Y\delta_R}$, $C_{K\delta_R}$, $C_{N\delta_R}$ are non-dimensional coefficients, V_B is the boat velocity, ρ_ω is the water density, L_{WL} is the length on design waterline, D_K is the design draft length, δ_R is the physical rudder angle and α_R is the effective angle of attack on the rudder as defined below

$$\alpha_R = \delta_R - \epsilon_y \gamma - \tan^{-1} \left(\frac{x_R R}{U} \right) \quad (4.7)$$

$$\epsilon = \frac{d\epsilon}{d\gamma} \times \gamma = \epsilon_\gamma \gamma \quad (4.8)$$

where γ is the leeway angle the sailboat is sailing and ϵ is the angle of inflow from the downwash generated by the keel and x_R is the longitudinal distance of the quarter-chord point of the rudder to the CG of the boat. The angles α_R , δ_R , γ and ϵ are illustrated in Figure 4.4

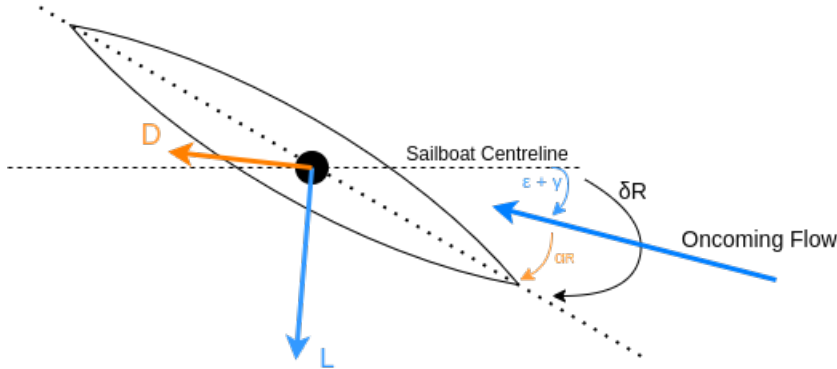


Figure 4.4: Definition of Rudder Angles

4.2. Sail Theory

4.2.1. Sail Theory and Terminology

Sail makers make use of their own language in naming for sails and sailboats [15]. It is important to know this language in order to have a conversation about sails. For instance the front of a sail is called the *bows* while the rear is called the *stern*. As shown in Figure 4.5 the *luff* is the leading edge of the sail and the *leech* is the trailing. The *foot* is the bottom edge which can be attached to the *boom* or left loose. Sails generally come to a point at the head, the attachment point to the mast at the top of the sail, but it is also common to see sails with a square top. The *tack* and the *clew* are the attachments points of the foot at the *luff* and *leech* respectively.

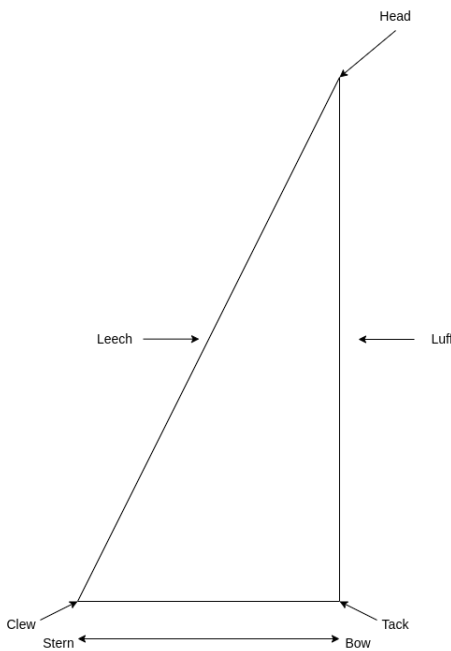


Figure 4.5: Naming convention of a sail

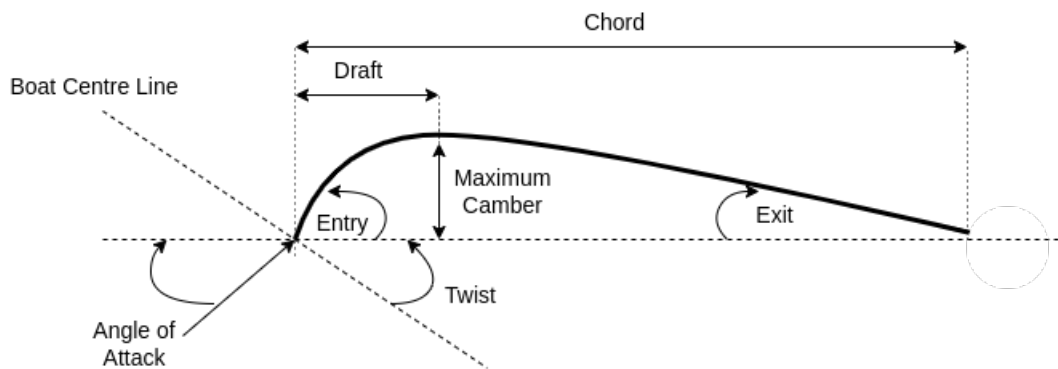


Figure 4.6: Terminology of a sail wing and shape

The shape of a sail can vary in its height and span and has almost no thickness, a horizontal section can be classified using the terminology of a wing. The terms are illustrated in Figure 4.6. The *chord* is the straight line between the leading and trailing edge. *Camber* is then the perpendicular distance from the chord line to the foil. *Draft* is the position of the maximum camber along the chord line. *Entry* and *exit* angles of the foil are, respectively, the angles of the leading and trailing edge to the chord line. *Angle of attack(AoA)* is the angle between the oncoming flow and the chord line and the *twist* angle is the angle between the chord line and the sailboat's centre line.

Depending on the tack of the boat, the side from which the wind is blowing from, illustrated in Figure 4.7, is the *windward* side and the other side will be *leeward* side.

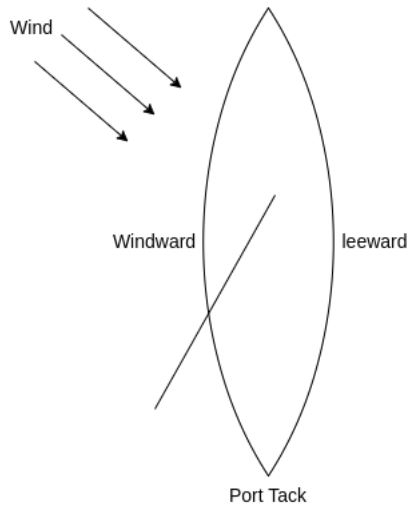


Figure 4.7: Windward and leeward definitions

4.2.2. Aerodynamics of a Sail

The way sail function, is much alike to that of a wing with some differences. Both a sail and a wing generate a force due to a pressure difference acting over their area. The three major differences between a sail and a wing are that a sail has almost no thickness, often has a large camber and generally operate at higher angles of attack. The flow around the sail is also usually disturbed by the mast or stays leading to large areas of separation as shown in [16]. Bernoulli's equation state that the pressure is inversely related to velocity and thus it can be seen through the contraction of the streamlines over the leeward side that the flow will accelerate creating a drop in pressure.

The simplified explanation of how lift is created due to the particles travelling further over the leeward side does not hold much substances for thin aerofoils such as sails. The way a airplane wing generates lift is due to the shape of the airfoil, the air flows faster over the top than it does over the bottom, because it has a further travel distance. With thin-airfoil sails the distance over the top and bottom is the same, so this the same reasoning for lift does not hold. By looking at the numerical solution of a flat plate, found in [17], gives insight to how a sail is affected by pressure. The first results, illustrated in Figure 4.8, showed that the thin-airfoil has no lift, which is incorrect.

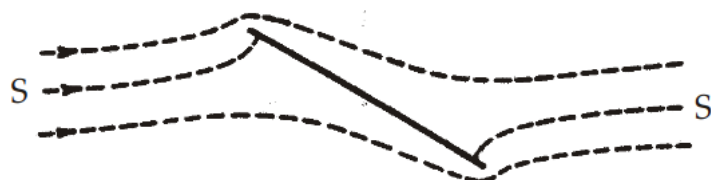


Figure 4.8: Flow field without circulation

Noting that these mathematical models determined streamlines that make very sharp turns in getting around the leading edge and trailing edge of the airfoil. For a thin airfoil this would mean infinite velocities, and to reduced these velocities the airfoil can be bent around the leading edge. For the flow at the trailing edge the assumption is made that the airflow will leave the airfoil smoothly in a direction determined by an imaginary slight extension of the airfoil, which is known as the Kutta condition. It has been found

that the Kutta condition can be satisfied mathematically by superimposing another type of flow solution, called circulation, onto the flat plate airfoil model. The superposition is shown in Figure 4.9.

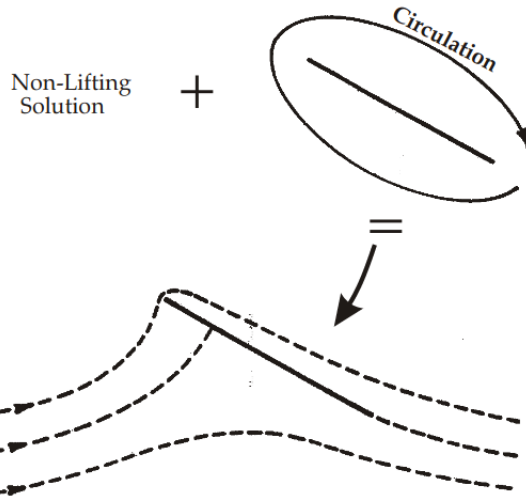


Figure 4.9: Superposition of circulation and non-circulation solution to give lift

Figure 4.10 illustrates the lift and drag component experienced due to wind on the sail. The drag component is always in the direction of the apparent wind and the lift is perpendicular to the apparent wind. γ_w is the apparent wind angle, α is the AoA of the sail wing, ψ is the leeway angle, which is the angle between the course and the heading, and θ is the sinusoidal angle between the net and lift force.

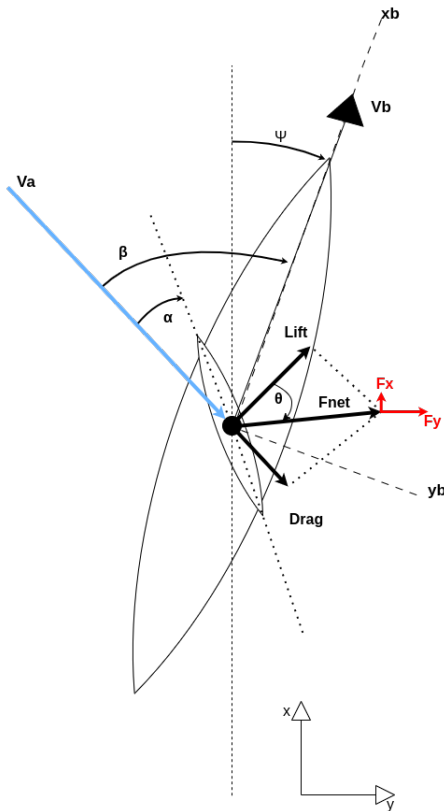


Figure 4.10: Lift and drag forces due to wind on sail wing

The lift and drag forces are defined by,

$$F_L = \frac{1}{2} C_L \rho U_A^2 A \quad (4.9)$$

$$F_D = \frac{1}{2} C_D \rho U_A^2 A \quad (4.10)$$

where C_L and C_D are the lift and drag coefficients, U_A the apparent wind speed, A area of the sail and ρ the air density. The lift and drag forces are combined into a single net aerodynamic force whose magnitude and angle relative to the apparent wind perpendicular defined as

$$|F_{net}| = F_{net} = \frac{1}{2} \rho U_A^2 A \sqrt{C_L^2 + C_D^2} \quad (4.11)$$

$$\theta = \tan^{-1} \left(\frac{C_D}{C_L} \right) \quad (4.12)$$

The component parallel to the direction of motion is the aerodynamic driving force F_x , while the force perpendicular to the direction of motion is the aerodynamic side force. Besides being a function of the angle of attack of the wing sail (θ is a function of α), F_x and F_y are both dependent on the apparent wind angle and the wind profile in which the vessel is sailing. F_x and F_y are defined below,

$$F_x = F_{net} \sin(\gamma_\omega - \theta) \quad (4.13)$$

$$F_y = F_{net} \cos(\gamma_\omega - \theta) \quad (4.14)$$

The equations above is valid for any lifting surface, whether it is a rigid wing sail or a cloth sail. For efficient performance of a sailing vehicle, the lifting surface will maximize the aerodynamic driving force while minimizing the aerodynamic side force. At a given leeway angle, the aerodynamic force ratio (F_x/F_y) is at a maximum when θ is minimized. In the limit that $C_D/C_L \rightarrow 0$, the aerodynamic force ratio approaches the limit $F_x/F_y \rightarrow \tan(\gamma_\omega)$

4.2.3. Sail Forces and Moments

The sail forces and moments are expressed in their horizontal components. When the sail is in the upright position the aerodynamic coefficients X'_{s0} and Y'_{s0} are expressed using lift coefficient L'_{s0} and drag coefficient D'_{s0} as shown in [18].

$$X'_{s0} = L'_{s0} \sin(\gamma_\omega) - D'_{s0} \cos(\gamma_\omega) \quad (4.15)$$

$$Y'_{s0} = L'_{s0} \cos(\gamma_\omega) + D'_{s0} \sin(\gamma_\omega) \quad (4.16)$$

where the subscript of 0 means value at the upright condition.

In the heeled condition, when the vessel is rotated due to the sail lift and drag force, the effect of the heel on the aerodynamic forces is produced by the reduction of both the apparent wind angle and apparent wind speed. The apparent wind angle in the heeled condition $\gamma_{\omega\phi}$ is expressed as follows using the apparent wind angle γ_ω and apparent wind speed U_A :

$$\gamma_{\omega\phi} = \tan^{-1} \left(\frac{U_A \sin(\gamma_\omega) \cos(\phi)}{U_A \cos(\gamma_\omega)} \right) = \tan^{-1} (\tan(\gamma_\omega) \cos(\phi)) \quad (4.17)$$

The apparent wind speed in the heeled condition $U_{A\phi}$ is also expressed as:

$$U_{A\phi} = \sqrt{((U_A \cos(\gamma_\omega))^2 + (U_A \sin(\gamma_\omega) \cos(\phi))^2} = U_A \sqrt{1 - (\sin(\gamma_\omega) \sin(\phi))^2} \quad (4.18)$$

For the close-hauled condition, tacking behaviour of sailboat due to not being able to sail directly into the wind, the sail may not stall due to the small attack angle. Therefore, the lift force will decrease proportionally to the reduction of both the apparent wind angle and the dynamic pressure of flow (square of the apparent wind speed). Hence the decreasing ratio of lift force by the heel angle ϕ can be described as:

$$\left(\frac{\gamma_{\omega\phi}}{\gamma_\omega} \right) \left(\frac{U_{A\phi}}{U_A} \right) = \left(\frac{\tan^{-1}(\tan(\gamma_\omega) \cos(\phi))}{\gamma_\omega} \right) (1 - (\sin(\gamma_\omega) \sin(\phi))^2) \quad (4.19)$$

The vector of lift force inclines with heel angle and rotates in the normal plane to the apparent wind axis. Since the angle between the apparent wind axis and the boat center line (heeling axis) is γ_ω , the rotating angle of the lift force vector ϕ' in the normal plane to the apparent wind axis is given by:

$$\phi' = \sin^{-1}(\cos(\gamma_\omega) \sin(\phi)) \quad (4.20)$$

Therefore, the decreasing ratio of horizontal component of the lift force is expressed as:

$$\left(\frac{\gamma_{\omega\phi}}{\gamma_\omega} \right) \left(\frac{U_{A\phi}}{U_A} \right) \cos(\phi') = \left(\frac{\tan^{-1}(\tan(\gamma_\omega) \cos(\phi))}{\gamma_\omega} \right) (1 - (\sin(\gamma_\omega) \sin(\phi))^2) \cos(\sin^{-1}(\cos(\gamma_\omega) \sin(\phi))) \quad (4.21)$$

Expanding the above mention equation in a power series and assuming that γ_A is small, results in

$$\left(\frac{\gamma_{\omega\phi}}{\gamma_\omega} \right) \left(\frac{U_{A\phi}}{U_A} \right) \cos(\phi') \approx \left(\cos^2(\phi) + \frac{1}{2} \sin^2(\phi) \right) \cos(\phi) = \frac{1}{2} (\cos(\phi) + \cos^3(\phi)) \quad (4.22)$$

Equation 4.22 can be further expanded in terms of ϕ and results in

$$\left(\frac{\gamma_{\omega\phi}}{\gamma_\omega} \right) \left(\frac{U_{A\phi}}{U_A} \right) \cos(\phi') \approx 1 - \phi^2 \quad (4.23)$$

Equation 4.23 is incidentally equal to the first two terms of the power series for the $\cos^2(\phi)$ function. Hence the curve of the $\cos^2(\phi)$ was compared with the calculated results in Equation 4.21 for three γ_ω cases. The calculated results show agreement with the curve of $\cos^2(\phi)$ in spite of the large γ_ω . Therefore, we adopted the formula of $\cos^2(\phi)$ to express the decreasing ratio of the horizontal component of the lift force in place of Equation 4.21.

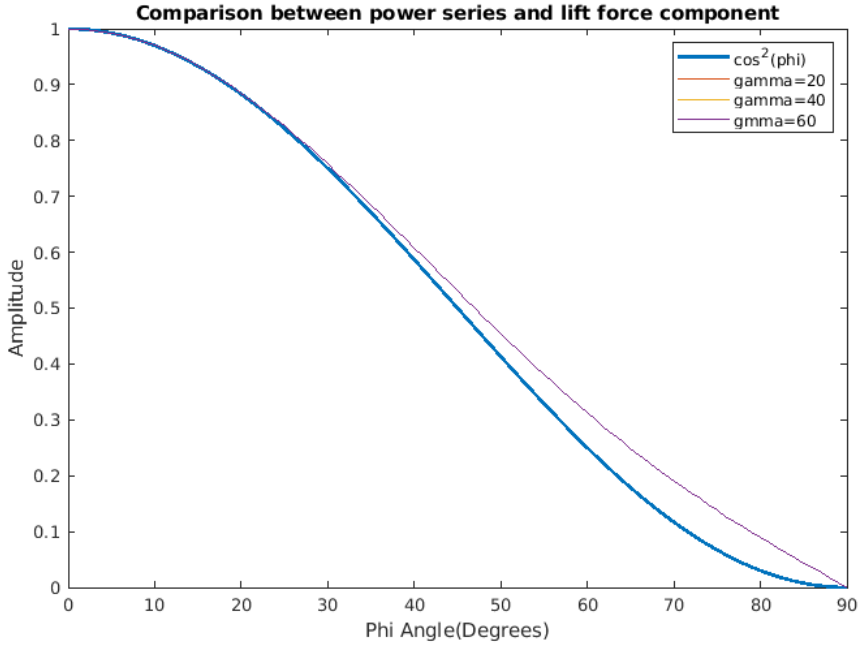


Figure 4.11: Lift force component represented as a power curve

Finally, when the lift coefficient represents the variation of the lift force including the contribution of dynamic pressure of apparent wind speed, the horizontal component of lift coefficient in the heeled condition L'_s is described as:

$$L'_s = L'_{s0} \cos^2(\phi) \quad (4.24)$$

The main part of the drag is caused by the induced drag, which is in proportion to the square of the lift force. The reduction of lift force expressed by Equation 4.19 is also approximated by $\cos(\phi)$. The vector of the drag force is in line with the apparent wind axis and does not incline by the heel angle. Therefore the horizontal component of the drag coefficient D'_s is described as:

$$D'_s = D'_{s0} \cos^2(\phi) \quad (4.25)$$

From these results, the aerodynamic coefficients in the horizontal components X'_s and Y'_s are then expressed as follows using the coefficients at the upright condition L'_{s0} and D'_{s0} :

$$X'_s = L'_s \sin(\gamma_\omega) - D'_s \cos(\gamma_\omega) = L'_{s0} \cos^2(\phi) \sin(\gamma_\omega) - D'_{s0} \cos^2(\phi) \cos(\gamma_\omega) = X'_{s0} \cos^2(\phi) \quad (4.26)$$

$$Y'_s = L'_s \cos(\gamma_\omega) - D'_s \sin(\gamma_\omega) = L'_{s0} \cos^2(\phi) \cos(\gamma_\omega) - D'_{s0} \cos^2(\phi) \sin(\gamma_\omega) = Y'_{s0} \cos^2(\phi) \quad (4.27)$$

The moment K_s is generated mainly by the Y_s force, however it is also affected by the component normal to the mast, hence

$$K'_s = -Y'_s \left(\frac{z_{GCE}^G}{\sqrt{S_A}} \right) / \cos(\phi) \quad (4.28)$$

where z_{GCE}^G is the z-coordinate of the geometric center of effort of the sail from the CG of the boat and negative upwards.

The moment N_s is also generated mainly by the Y_s force, however, it is well known that the N_s is also affected by the heel angle ϕ due to the application point of the thrust force X_s moving outboard to lee side. Therefore N'_s can be written, including the effect of X'_{s0} as

$$N'_s = \left(Y'_{s0} \frac{x_{GCE}^G}{\sqrt{S_A}} + X'_{s0} \frac{z_{GCE}^G}{\sqrt{S_A}} \sin(\phi) \right) \cos^2(\phi) \quad (4.29)$$

where x_{GCE}^G is x-coordinate of the geometric center of effort of the sail from CG of the boat.

The sail force and moment components defined above are shown below:

$$X_s = X'_{s0} \cos^2(\phi) \times \frac{1}{2} \rho_a U_A^2 S_A \quad (4.30)$$

$$Y_s = Y'_{s0} \cos^2(\phi) \times \frac{1}{2} \rho_a U_A^2 S_A \quad (4.31)$$

$$K'_s = -Y'_s \left(\frac{z_{GCE}^G}{\sqrt{S_A}} \right) / \cos(\phi) \times \frac{1}{2} \rho_a U_A^2 S_A \quad (4.32)$$

$$N'_s = \left(Y'_{s0} \frac{x_{GCE}^G}{\sqrt{S_A}} + X'_{s0} \frac{z_{GCE}^G}{\sqrt{S_A}} \sin(\phi) \right) \cos^2(\phi) \times \frac{1}{2} \rho_a U_A^2 S_A \quad (4.33)$$

Chapter 5

Guidance and Waypoint Navigation

This chapter presents the implementation of a guidance controller that controls a ocean vessel to a path consisting of a set of waypoints. It also discusses the generation of a path based on the waypoints and a straight path following control system.

5.1. Guidance System

The guidance system is similar to the aircraft guidance system, discussed in [19]. The defined guidance consists of a series of straight-line path segments between waypoints. Each waypoint is a set of North and East coordinates on a map. The straight line between two consecutive waypoints is defined as the ground track. The purpose of the guidance controller is to control the ocean vessel onto the ground track by controlling the cross-track position error to zero. Given that you have the source waypoint and the destination waypoint, the heading angle and the length of the ground track can be calculated as illustrated in Figure

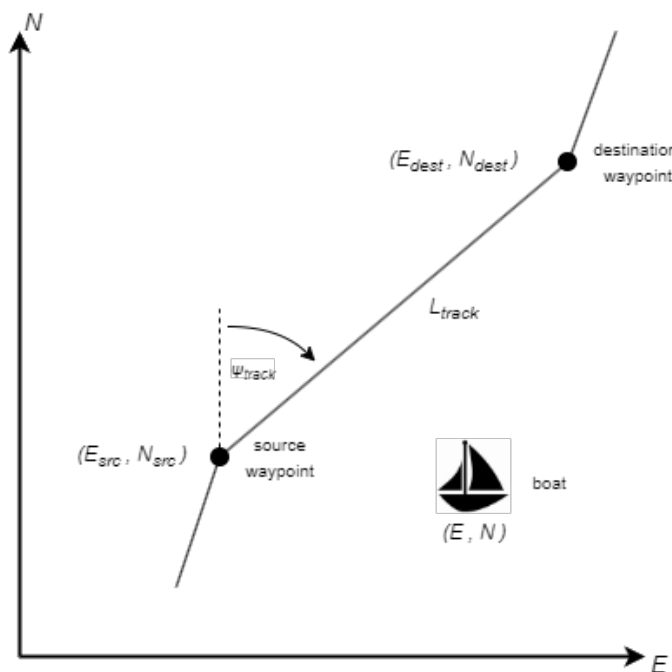


Figure 5.1: Ground track between source waypoint and destination waypoint

The track heading ψ_{track} and the track length L_{track} is calculated as

$$\psi_{track} = \tan^{-1} \left(\frac{E_{dest} - E_{src}}{N_{dest} - N_{src}} \right) \quad (5.1)$$

$$l_{track} = \sqrt{(N_{dest} - N_{src})^2 + (E_{dest} - E_{src})^2} \quad (5.2)$$

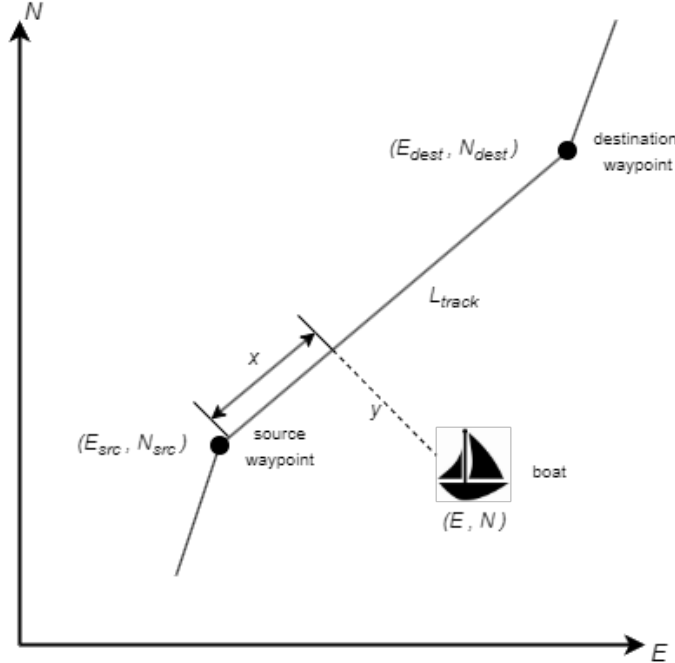


Figure 5.2: Cross-track error and in-track distance along track

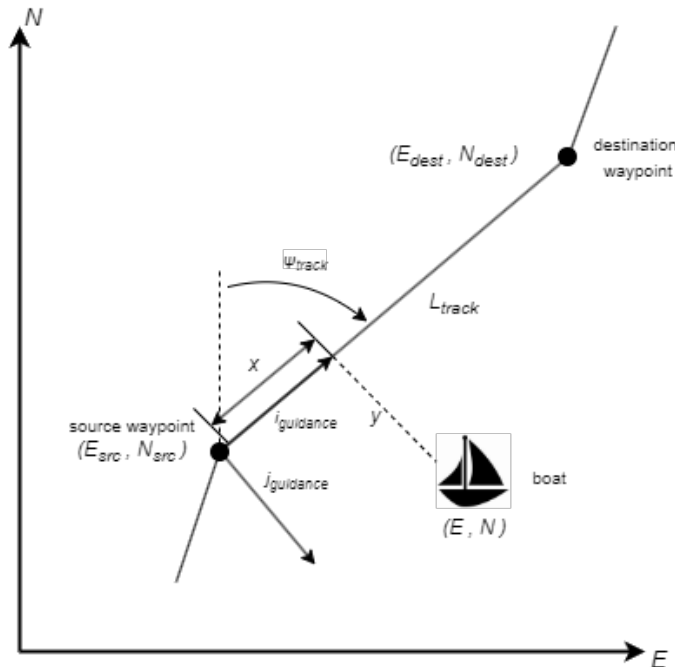


Figure 5.3: Guidance Axis System

The origin of the guidance axis system is at the location of the source waypoint, the x-axis is parallel to the ground track and pointing in the direction of the destination waypoint, its y-axis is perpendicular to the ground track, and its z-axis coincides with the down axis of the NED axis system. The guidance axis system is obtained by rotating the NED axis system through the track heading ψ_{track} , and by moving its origin to the location of the source waypoint.

To obtain the cross-track error and the in-track distance, the boat position is first transformed from the NED axes to the guidance axes. The cross-track error is then simply the y-component in the guidance axis system, and the in-track distance is simply the x-component in the guidance axis system. The boat's position is transformed from the NED axis system to the guidance axis system with the following equation

$$\begin{bmatrix} s \\ e \end{bmatrix} = \begin{bmatrix} \cos(\psi_{track}) & \sin(\psi_{track}) \\ -\sin(\psi_{track}) & \cos(\psi_{track}) \end{bmatrix} \begin{bmatrix} N - N_{src} \\ E - E_{src} \end{bmatrix} \quad (5.3)$$

The boat is following the ground track when the boat heading equals the ground track heading and the cross-track error is equal to zero. The boat will have reached the destination waypoint when its in-track distance equals the length of the ground track.

5.2. Straight path Generation based on Waypoints

For surface craft vessels, discussed in [7], only two coordinates (x_k, y_k) for $k = 1, \dots, n$. The waypoint database therefore consists of

$$wpt.pos = (x_0, y_0), (x_1, y_1), \dots, (x_n, y_n) \quad (5.4)$$

Additionally other waypoint properties such as speed and heading is defined as,

$$wpt.speed = U_0, U_1, \dots, U_n \quad (5.5)$$

$$wpt.heading = \psi_0, \psi_1, \dots, \psi_n \quad (5.6)$$

In the case of a sailboat the speed is dependent on the wind and therefor is not considered in the waypoint navigation. The states that are thus important for sailboats during navigation are (x_i, y_i, ψ_i) , which are called the *pose*. The heading angle is usually not important but in the case of a sailboat it is important due to the constraint on sailing angles especially when performing the tacking maneuvering, which is discussed in Chapter

In 1957 Dubins [20] found the shortest path for path following and can be summarised as, "The shortest path (minimum time) between two configurations (x, y, ψ) of a craft moving at constant speed U is a path formed by a straight lines and circular arc segments.". Since a craft is considered the start and end configurations are expressed in terms of positions (x, y) , heading angle ψ and in addition it is assumed there is bounds on the turning rate r . Although this method has drawbacks with a jump in turn rate, the use of arcs and straight lines is very simplistic. Figure 5.4 illustrates a path generated by the Dubins method. Also that needs to be considered is that the operator can specify a circle with radius R_i about each waypoint and can be stored in the database as

$$wpt.radius = R_0, R_1, \dots, R_n \quad (5.7)$$

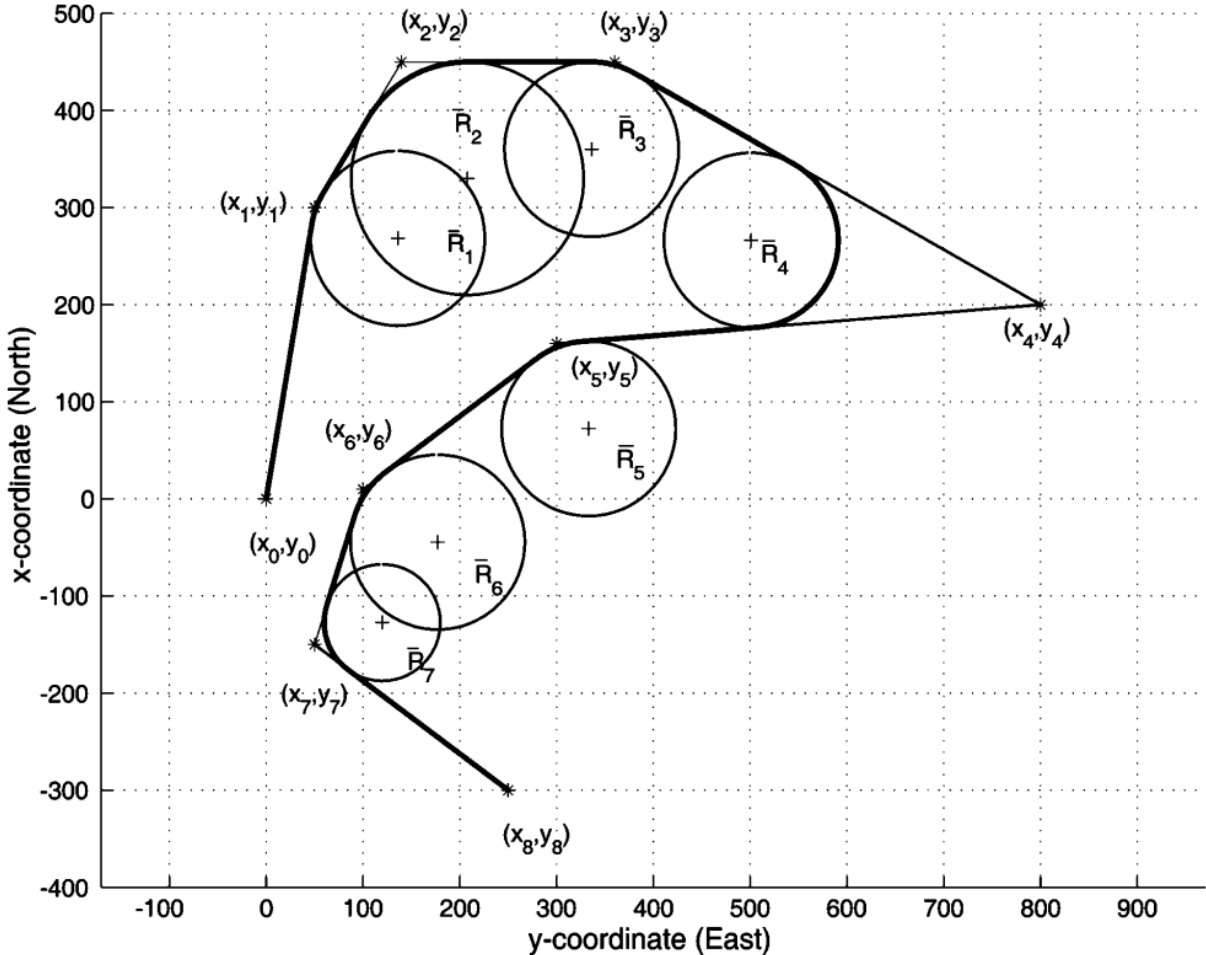


Figure 5.4: Straight lines and circular arc segments for waypoint guidance

5.3. Line-of-Sight (LOS) Steering Law

In order to steer the boat on a path a method known as the *lookahead – based steering* [21]. For path-following purposes, only the cross-track error is relevant since $e(t) = 0$ means that the boat has converged to the straight line. Thus the associated control objective for straight-line path following becomes

$$\lim_{t \rightarrow \infty} e(t) = 0 \quad (5.8)$$

For lookahead-based steering, the course angle assignment is separated into two parts:

$$x_d(e) = x_p + x_r(e) \quad (5.9)$$

where

$$x_p = \alpha_k \quad (5.10)$$

is the *path – tangential angle* illustrated in Figure 5.5, while

$$x_r(e) = \arctan\left(\frac{-e}{\Delta}\right) \quad (5.11)$$

is a *velocity-path relative angle*, which ensures that the velocity is directed toward a point on the path that is located a *lookahead distance* $\Delta(t) > 0$ ahead of the direct projection of $p^n(t)$ on to the path.

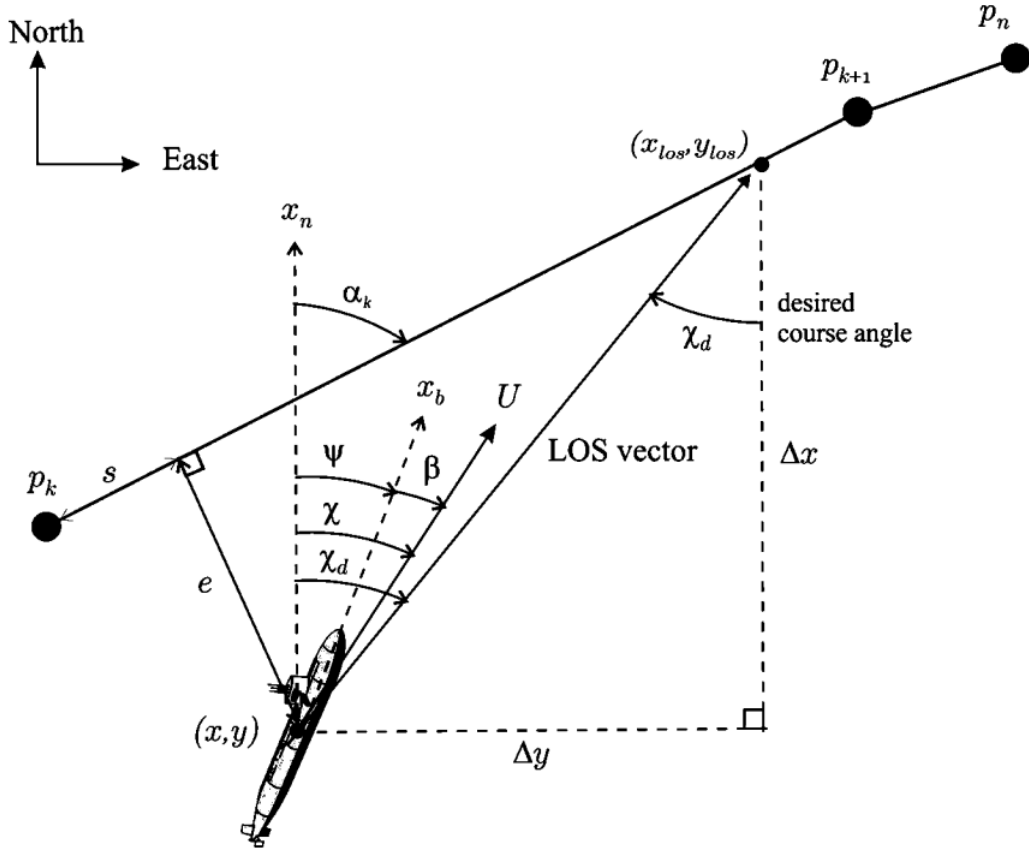


Figure 5.5: LOS guidance where the desired course angle x_d is chosen to point toward the LOS intersection point (x_{los}, y_{los})

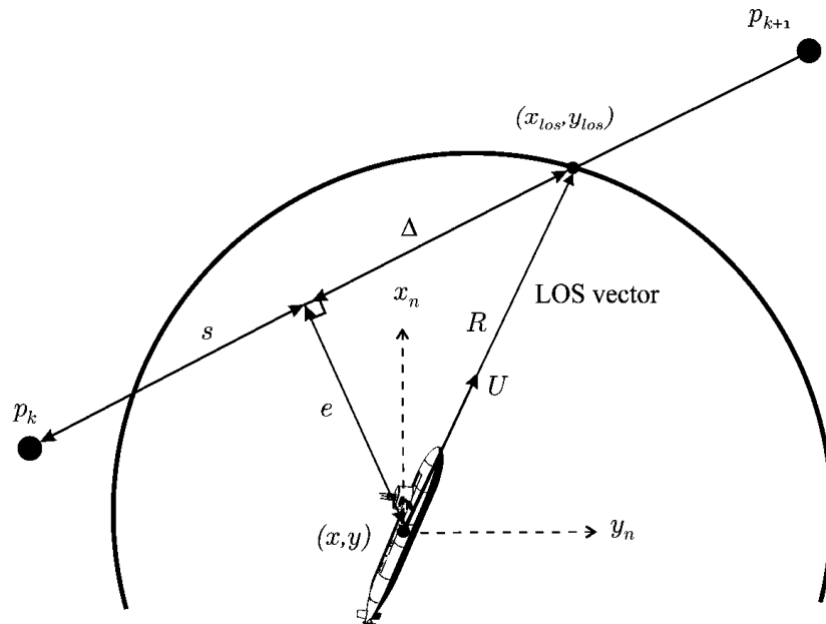


Figure 5.6: Circle of acceptance with constant radius R

Figure 5.6 illustrates that the circle of acceptance radius R is equal to

$$e(t)^2 + \Delta(t)^2 = R^2 \quad (5.12)$$

with

$$\Delta(t) = \sqrt{R^2 - e(t)^2} \quad (5.13)$$

varying between 0 and R for $|e(t)| = R$ and $|e(t)| = 0$, respectively. The steering law, in Equation 5.11, can also be interpreted as a saturating control law,

$$x_r(e) = \arctan(-K_p e) \quad (5.14)$$

where $K_p(t) = 1/\Delta(t) > 0$. Notice that the lookahead-based steering law is equivalent to a saturated proportional control law, effectively mapping $e \in R$ into $x_r(e) \in [-\pi/2, \pi/2]$. As shown in the geometry of Figure 5.6, a small lookahead distance implies aggressive steering, which intuitively is confirmed by a correspondingly large proportional gain in the saturated control interpretation. However because a sailboat is an underactuated vessel that can only steer by attitude information and is subject to influence like ocean currents and nonzero slip angles B . This suggest that a integral controller will be a needed for the sailboat to follow straight-line. The integral controller is shown below,

$$x_r(e) = \arctan \left(-K_p e - K_i \int_0^t e(\tau) d\tau \right) \quad (5.15)$$

with $K_i > 0$. Considering horizontal path following along straight lines, the desired yaw angle can be computed by,

$$x_d(e) = \alpha_k + x_r(e) \quad (5.16)$$

with $x_r(e)$ as in Equation 5.14. In practice, to avoid overshoot and windup affects, care must be taken when using integral action in the steering law. Specifically, the integral term should only be used when a steady-state off-track condition is detected.

5.4. Path-Following Controllers

The path-following controller depends on having access to velocity measurements. This methods aim is to align the velocity and LOS vector. The desired course angle x_d is computed such that the velocity vector is along the path(LOS vector) using the *lookahead-based steering* law,

$$x_d(e) = x_p + x_r(e) = \alpha_k + \arctan(-K_p e) \quad (5.17)$$

The control objective $x \rightarrow x_d$ is satisfied by transforming the course angle command x_d to a heading angle command ψ_d . This requires the knowledge of the β since, illustrated in Figure 5.7,

$$\psi_d = x_d - \beta \quad (5.18)$$

The velocity and LOS vectors can be aligned using a heading controller, discussed in Chapter 7, with the following error signal,

$$\psi = \psi - \psi_d = \psi - x_d + \beta \quad (5.19)$$

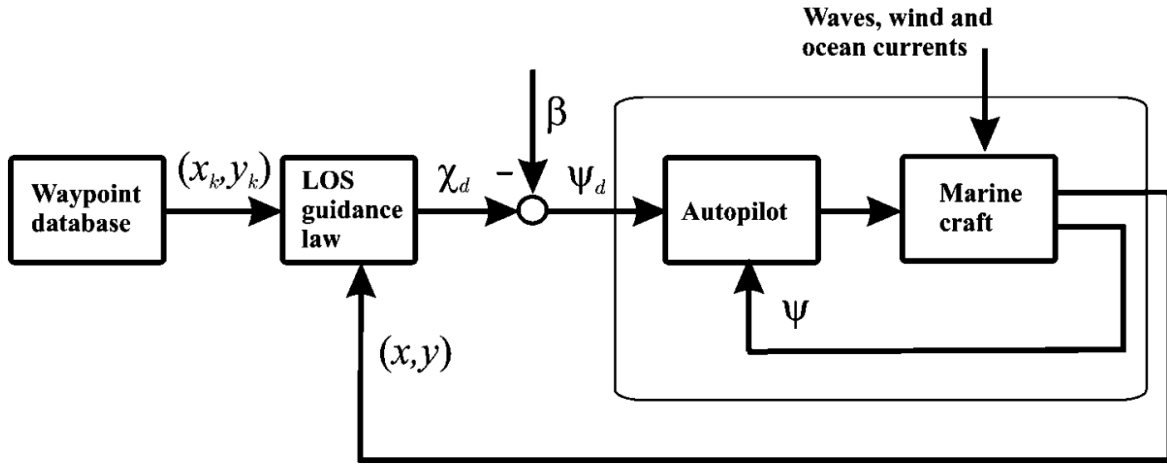


Figure 5.7: LOS guidance principle where the side slip angle β can be applied and compensated for by using integral action

If the velocities of the vessel are measured, the sideslip angle can be computed by

$$\beta = \arcsin\left(\frac{v}{U}\right) \quad (5.20)$$

Guidance laws of PI type avoid velocity measurements by treating β as an unknown slowly varying disturbance satisfying $\beta \approx 0$.

5.5. Circle of Acceptance for Surface Vessel

When a vessel is traveling along a straight line piece wise path, made up of n straight-line segments connected by $n + 1$ waypoints. A mechanism is required for selecting the next waypoint. The next waypoint (x_{k+1}, y_{k+1}) can be selected on the basis of whether or not the vessel lies within a *circle of acceptance* with radius R_{k+1} around (x_{k+1}, y_{k+1}) . This means that the vessel position must at time t satisfy,

$$[x_{k+1} - x(t)]^2 + [y_{k+1} - y(t)]^2 \leq R_{k+1}^2 \quad (5.21)$$

then the next waypoint (x_{k+1}, y_{k+1}) should be selected. A suggested method is to select the radius R depending on the distance between the two waypoints.

$$R = b \frac{y_{k+1} - y_k}{x_{k+1} - x_k} \quad (5.22)$$

where the value b is a constant value.

Chapter 6

Fundamental Properties of Linear steering dynamic model

The state space model associated with the first order Nomoto model is both observable and controllable. The state space model associated with the second order Nomoto model is also observable, however it is controllable only if the effective sway time constant is different from the effective yaw time constant. The first order model is very popular in adaptive autopilot applications. Model reduction for a fourth order transfer function ship model describing the sway-yaw-roll dynamics is conducted to reach the second order Nomoto model describing the sway-yaw dynamics and the first order Nomoto model describing the yaw dynamics itself.

6.1. Ship Steering Dynamics Model Reduction

For ship autopilots design, a simple model with average predicting capability is usually preferred. Based on the linearized surge-sway-yaw-roll equations of motion, a fourth order transfer function relating the yaw rate to the rudder angle is derived.

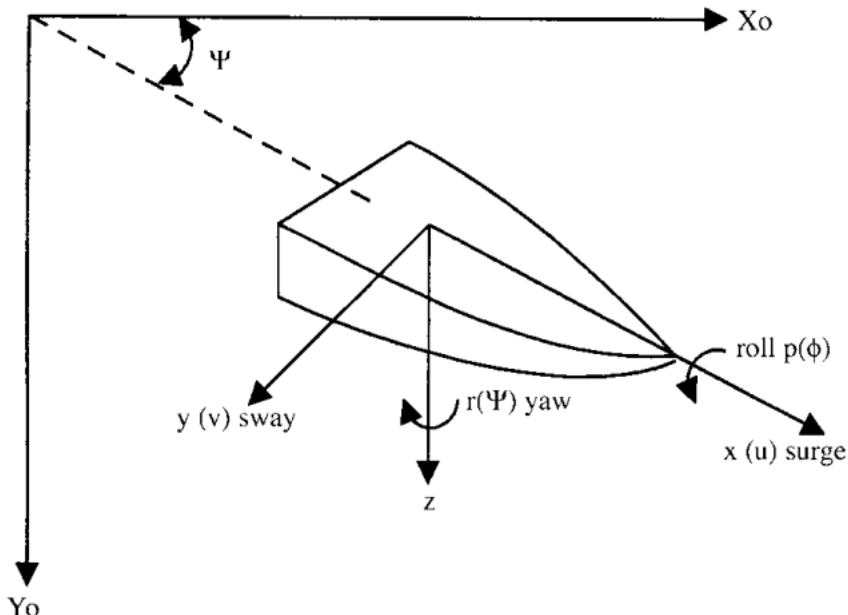


Figure 6.1: Sway-yaw-roll motion coordinate system

Upon linearization with respect to a straight line motion with a constant forward speed u_0 , the surge

equation is decoupled and the following linear coupled sway-yaw-roll equations follow,

$$m(\dot{v} + u_0 r) = Y_v V + Y_{\dot{v}} \dot{V} + Y_\phi \phi + Y_p P + Y_{\dot{P}} \dot{P} + Y_r r + Y_{\dot{r}} \dot{r} + Y_\delta \delta \quad (6.1)$$

$$I_X \ddot{\phi} = K_v V + K_{\dot{v}} \dot{V} + Y_\phi \phi + K_p P + K_{\dot{P}} \dot{P} + K_r r + K_{\dot{r}} \dot{r} + K_\delta \delta - mgGM\phi \quad (6.2)$$

$$I_z \ddot{\psi} = N_v V + N_{\dot{v}} \dot{V} + N_\phi \phi + N_p P + N_{\dot{P}} \dot{P} + N_r r + N_{\dot{r}} \dot{r} + N_\delta \delta \quad (6.3)$$

where Y_v , $Y_{\dot{v}}$, ... indicate the hydrodynamic coefficients; for instance Y_v indicates the derivative of the sway force Y to the sway speed V evaluated at the reference condition; m is the mass of the ship; I_x is the moment of inertia about the x-axis; I_z is the moment of inertia about the z-axis; V is the sway speed; u is the surge speed; r is the yaw rate; ψ is the heading angle defined by $\dot{\psi} = r$; p is the roll rate; ϕ is the roll angle defined by $\dot{\phi} = p$ and GM is the metacentric height, which indicates the restoring capability of a ship in rolling motion. Taking the Laplace transform of Equations 6.1-3 and rearranging, we have

$$a_1 V = a_2 \Phi + a_3 r + a_4 \delta \quad (6.4)$$

$$b_1 \Phi = b_2 V + b_3 r + b_4 \delta \quad (6.5)$$

$$c_1 r = c_2 V + c_3 \Phi + c_4 \delta \quad (6.6)$$

where

$$a_1 = m - Y_{\dot{v}} S - Y_v \quad (6.7)$$

$$a_2 = Y_{\dot{P}} S^2 + Y_p S + Y_\phi \quad (6.8)$$

$$a_3 = Y_{\dot{r}} S + Y_r + mu_0 \quad (6.9)$$

$$a_4 = Y_\delta \quad (6.10)$$

$$b_1 = (I_X - K_{\dot{P}}) S^2 - K_p S + mgGM \quad (6.11)$$

$$b_2 = K_{\dot{v}} S + K_v \quad (6.12)$$

$$b_3 = K_{\dot{r}} S + K_r \quad (6.13)$$

$$b_4 = K_\delta \quad (6.14)$$

$$c_1 = (I_Z - N_{\dot{r}}) S - N_r \quad (6.15)$$

$$c_2 = N_{\dot{v}} S + N_v \quad (6.16)$$

$$c_3 = N_{\dot{P}} S^2 + N_p S + N_\phi \quad (6.17)$$

$$c_4 = N_\delta \quad (6.18)$$

After eliminating the sway speed V and roll angle ϕ from Equations 6.4-6, the following transfer function relating the yaw rate r to the rudder angle δ can be obtained:

$$\frac{r}{\delta} = \frac{a_1(b_1c_4 + b_4c_3) + a_2(b_4c_2 - b_2c_4) + a_4(b_1c_2 + b_2c_3)}{a_1(b_1c_1 - b_3c_3) - a_2(b_2c_1 + b_3c_2) - a_3(b_1c_2 + b_2c_3)} \quad (6.19)$$

It can be easily verified that the numerator of Equation 6.19 is third order in S, while the denominator is fourth order in S. Hence, Equation 6.19 can be expressed in the following form.

$$\frac{r}{\delta} = \frac{K(1 + T_3S)(S^2 + 2n\omega_0S + w_0^2)}{(1 + T_1S)(1 + T_2S)(S^2 + 2\delta\omega_nS + w_n^2)} \quad (6.20)$$

where the quadratic factors are due to the coupling effect from the roll mode on the yaw rate. The zero ($1 + T_3S$) and the pole ($1 + T_2S$) are due to the coupling effect from the sway mode on the yaw dynamics. If the roll mode is neglected, Equation 7.8 can be further reduced to the following form

$$\frac{r}{\delta} = \frac{K(1 + T_3S)}{(1 + T_1S)(1 + T_2S)} \quad (6.21)$$

Equation 6.21 is known as the second order Nomoto model, where K is the static yaw rate gain, and T_1 , T_2 and T_3 are time constants. Numerical values of the parameters in Equation 6.21 for a Mariner class vessel are given by $T_1 = 118$, $T_2 = 7.8$, $T_3 = 18.5$ and $K = 0.185$. The zero term ($1 + T_3S$) and the high frequency pole term ($1 + T_2S$) are due to the coupling effect from the sway mode. In practice, because the pole term ($1 + T_2S$) and the zero term ($1 + T_3S$) in Equation 6.21 nearly cancel each other, a further simplification can be done to give first order Nomoto model

$$\frac{r}{\delta} = \frac{K}{(1 + TS)} \quad (6.22)$$

where

$$T = T_1 + T_2 - T_3 \quad (6.23)$$

in Equation 6.23 is called the effective yaw rate time constant. It is obtained by equating the right hand side of Equation 6.21 to the right hand side of Equation 7.9 requiring the equality relationship to hold up to first order in S. If $T_2 = T_3$; namely, a perfect cancellation occurs, then the equality relationship is true up to second order in S, then T is of course, equal to T_1 . For the Mariner class vessel, the value of the effective constant T in Equation 6.23 is given by $T = 107.3$.

The first order Nomoto model defined by Equation 7.9 is widely employed in the ship steering autopilot design. The yaw dynamics is characterized by the parameters K and T , which can be easily identified from standard maneuvering tests. In practice, ship steering autopilots are designed for heading angle control. Hence, it is the transfer function relating the heading angle ψ to the rudder angle δ being needed in the autopilot design. Since the yaw rate r is actually the time derivative of ψ , the required transfer function can be readily obtained by adding an integrator $\frac{1}{s}$ to the transfer function models defined by Equation 6.21 and Equation 7.9.

6.2. First Order Nomoto Model

The controllability, observability and identifiability properties of the first order Nomoto model-based system will be discussed in this section. The identifiability property will be discussed with respect to the first order Nomoto transfer function model. However, the controllability and observability properties have to be discussed with respect to the state-space model derived from the Nomoto model. This is because the transfer function model always represents the observable and controllable parts of the system

dynamics. If there is any unobservable or uncontrollable parts of the dynamics, they are cancelled out before reaching the transfer function model form. Hence, it only makes sense to discuss the controllability and observability properties of the state space model, which contains the observable, controllable and uncontrollable modes. Equation 7.9 can be expressed in time domain as

$$T\ddot{r} + r = K\delta \quad (6.24)$$

with the notation

$$\dot{\psi} = r \quad (6.25)$$

where ψ is the heading of the ship. Equation 6.24 can be written as

$$T\ddot{\psi} + \dot{\psi} = K\delta \quad (6.26)$$

Equation 6.25 and 6.26 can be arranged in the standard state space form

$$\dot{x} = Ax + Bu \quad (6.27)$$

$$y = Cx + du \quad (6.28)$$

where

$$x = \begin{bmatrix} \psi \\ r \end{bmatrix} \quad (6.29)$$

$$u = \delta \quad (6.30)$$

$$y = \psi \quad (6.31)$$

and

$$A = \begin{bmatrix} 0 & 1 \\ 0 & -\frac{1}{T} \end{bmatrix} \quad (6.32)$$

$$B = \begin{bmatrix} 0 \\ \frac{K}{T} \end{bmatrix} \quad (6.33)$$

$$C = \begin{bmatrix} 1 & 0 \end{bmatrix} \quad (6.34)$$

The first order system is both controllable and observable. Consequently, the first order Nomoto model satisfies the identifiability property, hence, on-line estimation of the model parameters based on the measured rudder and yaw rate information will be possible and adaptive control strategy can be successfully implemented.

6.3. Second Order Nomoto Model

The second order model Nomoto model is obtained by neglecting the roll mode. Namely,

$$m(\dot{v} + u_0 r) = Y_v V + Y_{\dot{v}} \dot{V} + Y_\phi \phi + Y_p P + Y_{\dot{P}} \dot{P} + Y_r r + Y_{\dot{r}} \dot{r} + Y_\delta \delta \quad (6.35)$$

$$I_z \dot{r} = N_v V + N_{\dot{v}} \dot{V} + N_\phi \phi + N_p P + N_{\dot{P}} \dot{P} + N_r r + N_{\dot{r}} \dot{r} + N_\delta \delta \quad (6.36)$$

The above equations can be put in state space format as

$$\begin{bmatrix} m - Y_{\dot{v}} & -Y_{\dot{r}} & 0 \\ -N_{\dot{v}} & I_z - N_r & 0 \\ 0 & 0 & 1 \end{bmatrix} \begin{bmatrix} \dot{v} \\ \dot{r} \\ \dot{\psi} \end{bmatrix} + \begin{bmatrix} -Y_v & mu_0 - Y_r & 0 \\ -N_v & I_z - N_r & 0 \\ 0 & 1 & 0 \end{bmatrix} \begin{bmatrix} v \\ r \\ \psi \end{bmatrix} = \begin{bmatrix} Y_\delta \\ N_\delta \\ 0 \end{bmatrix} \delta \quad (6.37)$$

In standard state space format,

$$x = \begin{bmatrix} v \\ r \\ \psi \end{bmatrix} \quad (6.38)$$

$$u = \delta \quad (6.39)$$

$$y = \psi \quad (6.40)$$

and

$$A = \begin{bmatrix} a_{11} & a_{12} & 0 \\ a_{21} & a_{22} & 0 \\ 0 & 1 & 0 \end{bmatrix} \quad (6.41)$$

$$B = \begin{bmatrix} b_{11} \\ b_{21} \\ 0 \end{bmatrix} \quad (6.42)$$

$$C = \begin{bmatrix} 0 & 0 & 1 \end{bmatrix} \quad (6.43)$$

The elements in matrix A and B are given by

$$a_{11} = \frac{(I_z - N_r)Y_v + Y_r N_v}{(m - Y_{\dot{v}})(I_z - N_r) - N_{\dot{v}} Y_{\dot{r}}} \quad (6.44)$$

$$a_{12} = \frac{(I_z - N_r)(Y_v - mu_0) + Y_r N_r}{(m - Y_{\dot{v}})(I_z - N_r) - N_{\dot{v}} Y_{\dot{r}}} \quad (6.45)$$

$$a_{21} = \frac{(m - Y_{\dot{v}})N_v + N_{\dot{v}} Y_v}{(m - Y_{\dot{v}})(I_z - N_r) - N_{\dot{v}} Y_{\dot{r}}} \quad (6.46)$$

$$a_{22} = \frac{(m - Y_{\dot{v}})N_r + N_{\dot{v}}(Y_v - mu_0)}{(m - Y_{\dot{v}})(I_z - N_r) - N_{\dot{v}} Y_{\dot{r}}} \quad (6.47)$$

$$b_{11} = \frac{(I_z - N_r)N_\delta + Y_r N_\delta}{(m - Y_{\dot{v}})(I_z - N_r) - N_{\dot{v}} Y_{\dot{r}}} \quad (6.48)$$

$$b_{21} = \frac{(m - Y_{\dot{v}})N_\delta + N_{\dot{v}} N_\delta}{(m - Y_{\dot{v}})(I_z - N_r) - N_{\dot{v}} Y_{\dot{r}}} \quad (6.49)$$

The second order Nomoto model based system is controllable if the following is true

$$a_{12}b_{21} - a_{22}b_{11} \neq b_{11}(a_{21}b_{11} - a_{11}b_{21}) \quad (6.50)$$

The sway to rudder transfer function is shown below,

$$\frac{v}{\delta} = \frac{K_v(1 + T_v S)}{(1 + T_1 S)(1 + T_2 S)} \quad (6.51)$$

where K_v is the static sway gain coefficient and T_v is the sway time constant. It is to be noted that the poles of the sway-rudder model defined by Equation 6.52 are exactly the same as those in the yaw-rudder model defined by Equation 7.8.

From Equation 7.8 and 6.52 it follows that

$$\frac{v}{r} = \frac{K_v(1 + T_v S)}{K(1 + TS)} \quad (6.52)$$

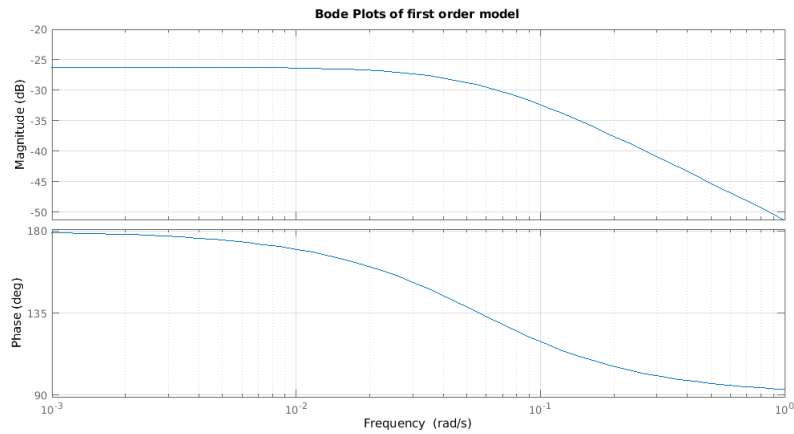
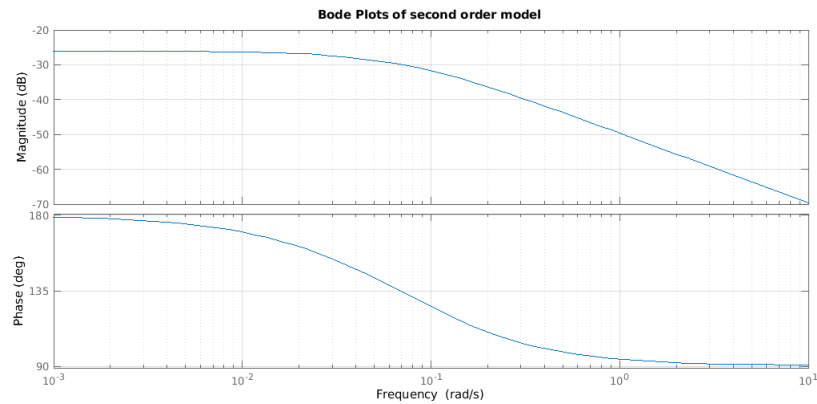
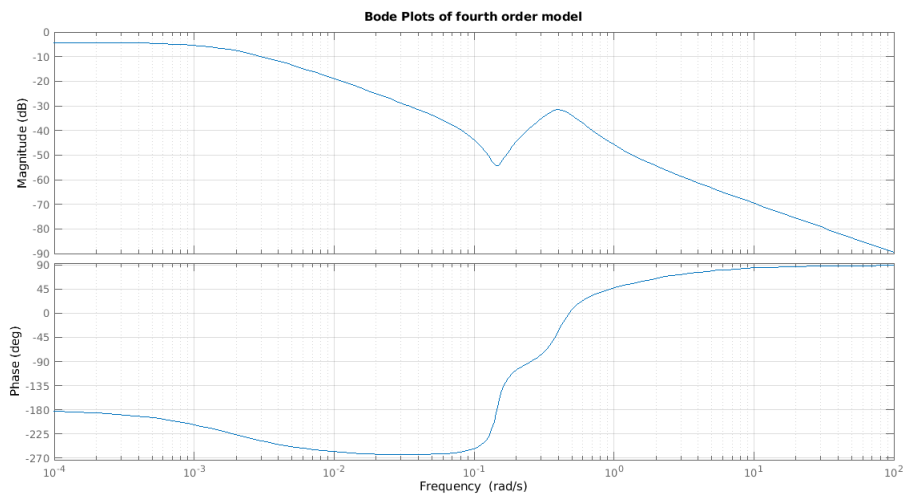
Equation 6.52 shows that if $T_v = T$, then v is proportional to r . Namely, v is dependent on r , since K_v/K is a constant. If the system is controllable, then the state variables ψ , r and v have to be able to move independently via application of the rudder angle δ . It is thus inferred that for the system to be controllable, T_v must be different from T . Namely $T_v \neq T$ is equivalent to the condition given in Equation 6.50 that ensures the controllability of the system. The system is observable, this implies that all the states (ψ, r, v) can be reconstructed from the measured heading angle ψ .

Identifiability of the second order Nomoto model implies that the parameters K , T_1 , T_2 and T_3 can be uniquely determined from the input δ and output r measurements. It is clear that if $T_2 = T_3$, then it is impossible to identify all the four parameters K , T_1 , T_2 and T_3 . Since the zero term $(1 + T_3 S)$ will cancel out the pole term $(1 + T_2 S)$. It is then inferred that the system is identifiable if $T_2 \neq T_3$.

In practice, the value of T_2 is nearly equal to the value of T_3 and we have a near cancellation situation. This will result in an ill-condition problem when trying to identify the values of T_2 and T_3 appearing in the second order Nomoto model. Due to this ill-condition property, the first order Nomoto model is preferred in the design for an adaptive autopilot, where reliable on-line estimation of the model parameters is needed.

6.4. Conclusion

The first order Nomoto model being very popular in the design for ship steering autopilots is not without reason. Its simplicity and reasonable accuracy in describing small rudder angle yaw dynamics make it attractive. Moreover, the relative easiness in identifying the model parameters makes it suitable for adaptive autopilot application, where on-line estimation of the model parameters is important. The second order Nomoto model includes the coupling effect from the sway to the yaw mode. This introduces a zero and a high frequency pole into the transfer function. The zero structure contributes to the overshoot phenomenon, which can be seen in the yaw rate for large rudder angle maneuvers. However, the ill-conditioning problem associated with the second order Nomoto model in the identification of the model parameters from input-output data seems to outweigh the improvement gained in its modeling capability. An approach that retains the zero structure while avoiding the ill-conditioning problem during on-line estimation has been proposed. The bode plots of the first, second and fourth order model is shown below,

**Figure 6.2:** First Order bode Plot**Figure 6.3:** Second Order Bode Plot**Figure 6.4:** Fourth Order Bode Plot

Chapter 7

Control of USV

This chapter takes a look at models for ocean vessels to control the heading, maneuvering and dynamic positioning. The chapter first looks at independently controlling the steering through the use of a rudder. The chapter considers the use of a linear and non-linear heading controller. The non-linear controller has advantages in the form of better heading control with small heading errors compared to the linear controller. The references angles for the sail and rudder on the sailboat is illustrated in the figure below,

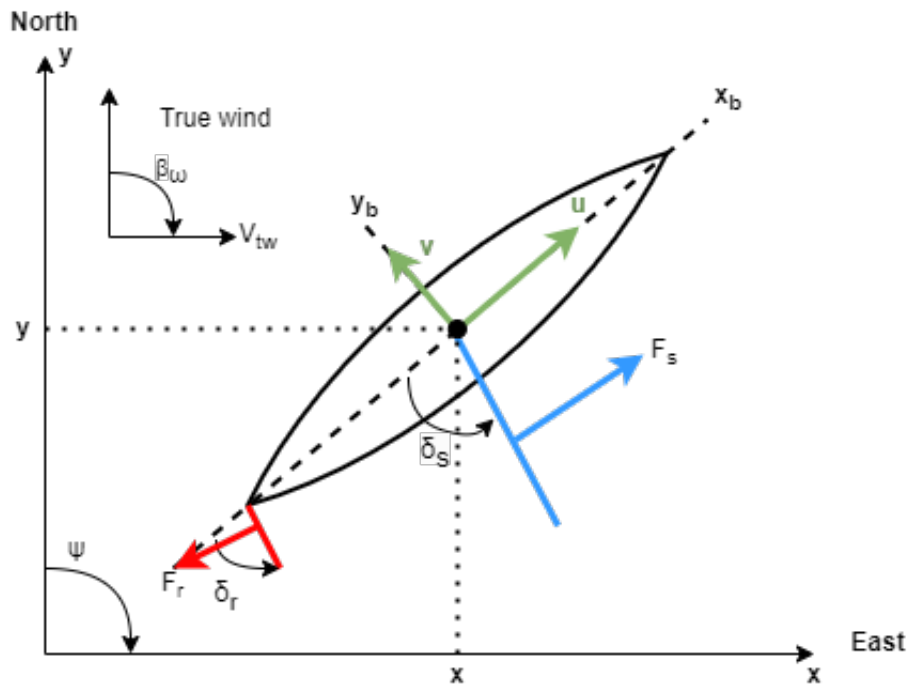


Figure 7.1: Reference angles of sailboat

7.1. Ocean Vessel Steering Control

A very popular approach in autopilot design is using the Nomoto model, which is based on the linearized surge-sway-yaw-roll equations. These equations are used to relate the yaw rate to the rudder angle. Upon linearization with respect to a straight line of motion with a constant forward speed u_0 , the surge equation is decoupled and the following linear coupled sway-yaw-roll equation is obtained, first in matrix form

$$M\dot{v} + N(u_0)v + Gn = \tau \quad (7.1)$$

where $v = [v, p, r]^T$, $n = [E, \phi, \psi]^T$, τ is the control vector. Assume that $I_{xy} = I_{yz} = 0$ and

$y_g = z_g = x_g = 0$. The matrix M is,

$$M = \begin{bmatrix} m - Y_v & -Y_{\dot{p}} & -Y_{\dot{r}} \\ K_v & I_x - K_{\dot{p}} & -I_{xz} - K_{\dot{r}} \\ -N_v & I_{xz} - N_{\dot{p}} & I_z - N_{\dot{r}} \end{bmatrix} \quad (7.2)$$

The matrix $N(u_0)$ is the matrix $C(v)$ and $D(v)$ linearised at constant speed u_0 ,

$$N(u_0) = \begin{bmatrix} -Y_v & -Y_p & mu_0 - Y_r \\ -K_v & -K_p & -K_r \\ -N_v & -N_p & -N_r \end{bmatrix} \quad (7.3)$$

and

$$G = \text{diag}(0, wGM_T, 0) \quad (7.4)$$

where $w=mg$, $\dot{\phi} = p$ and $\dot{\psi} \approx r$. Writing Equation 7.1 in difference equations results in,

$$m(\dot{v} + u_0 r) = Y_v V + Y_{\dot{v}} \dot{V} + Y_\phi \phi + Y_p P + Y_{\dot{p}} \dot{P} + Y_r r + Y_{\dot{r}} \dot{r} + Y_\delta \delta \quad (7.5)$$

$$I_X \ddot{\phi} = K_v V + K_{\dot{v}} \dot{V} + Y_\phi \phi + K_p P + K_{\dot{p}} \dot{P} + K_r r + K_{\dot{r}} \dot{r} + K_\delta \delta - mgGM\phi \quad (7.6)$$

$$I_z \ddot{\psi} = N_v V + N_{\dot{v}} \dot{V} + N_\phi \phi + N_p P + N_{\dot{p}} \dot{P} + N_r r + N_{\dot{r}} \dot{r} + N_\delta \delta \quad (7.7)$$

The transfer function relating the yaw rate to rudder angle is shown below,

$$\frac{r}{\delta} = \frac{K(1 + T_3 S)(S^2 + 2n\omega_0 S + w_0^2)}{(1 + T_1 S)(1 + T_2 S)(S^2 + 2\delta\omega_n S + w_n^2)} \quad (7.8)$$

When designing the controller the first order transfer function of yaw rate to rudder angle is used. The ocean vessel used in this case is a marine class vessel. The first order model is shown below,

$$\frac{r}{\delta} = \frac{K}{(1 + TS)} \quad (7.9)$$

It makes more sense to compare the rudder angle δ with the heading angle ψ . To obtain this transfer function multiply the transfer function mentioned above with an integrator $\frac{1}{S}$ and also substituting in the values for K and T_S results in,

$$\frac{\psi}{\delta} = \frac{-0.049}{(1 + 17.78S)S} \quad (7.10)$$

By analyzing the root locus plot of Equation 7.10. The root locus has two poles, one at $S = -0.0566$ and one at $S = 0$. From the root locus plot in Figure 7.2 it clear as the gain k increases the system will become unstable.

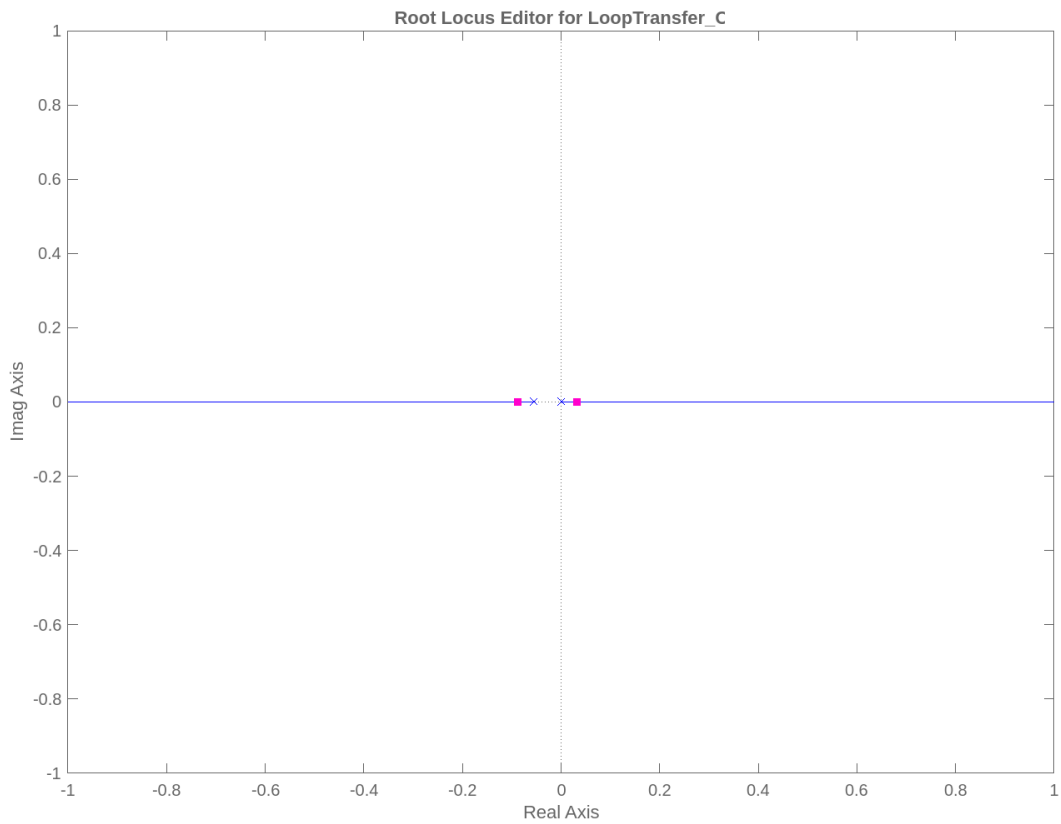


Figure 7.2: Root locus of first order system

7.1.1. Linear Rudder Control

In order to first stabilize the system the transfer function should be multiplied with a negative to invert the root locus, meaning only a negative gain should be used. The new root locus plot is illustrated in Figure 7.3. From the newly constructed root locus plot the system will be stable for any value of k . For $k = -1$, two complex poles at $s = -0.02811 \pm j * 0.0443$. The damping $\delta_d = 0.563$ and the natural frequency is $\omega_n = 0.0525$.

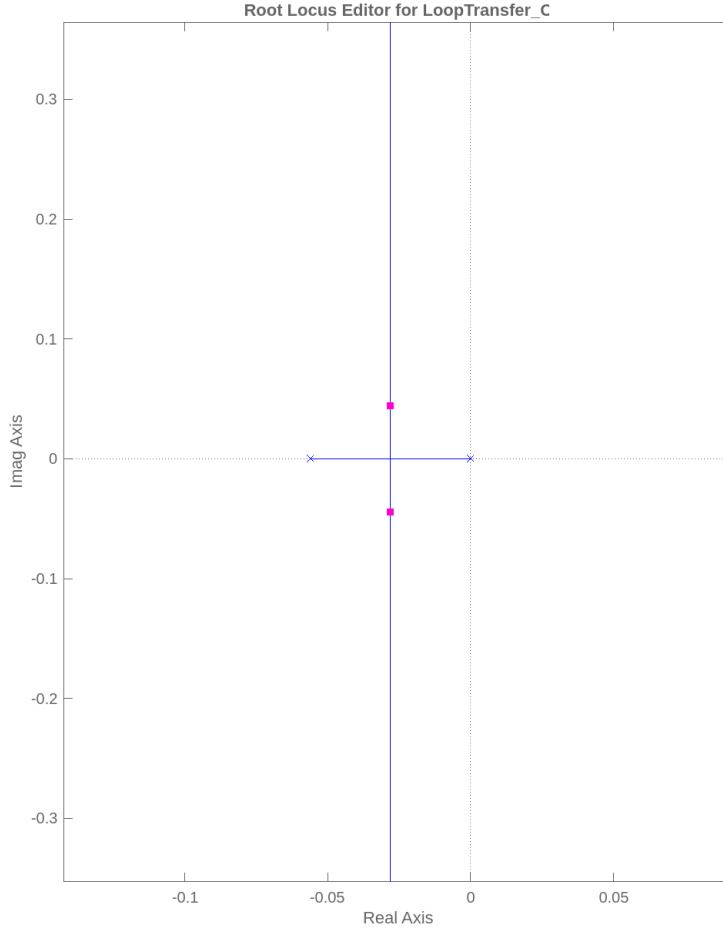
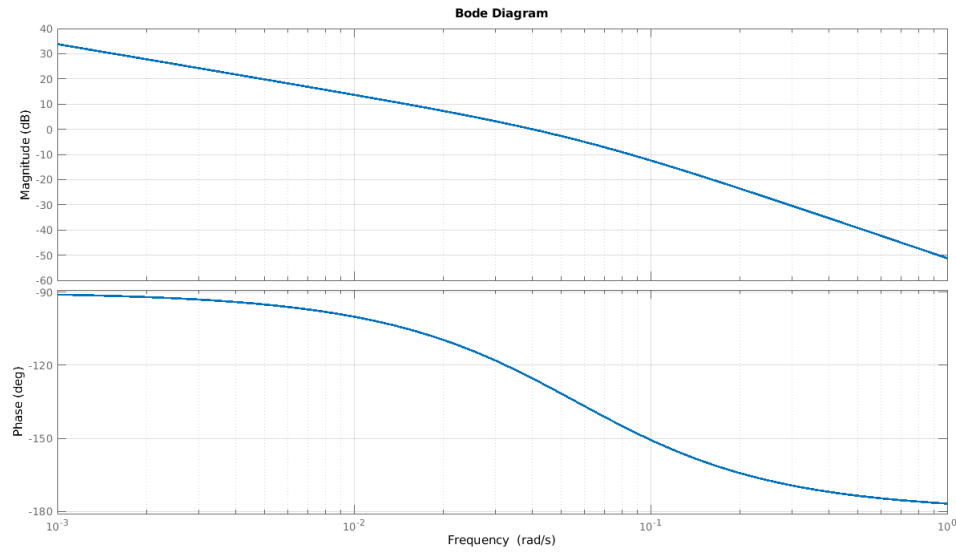
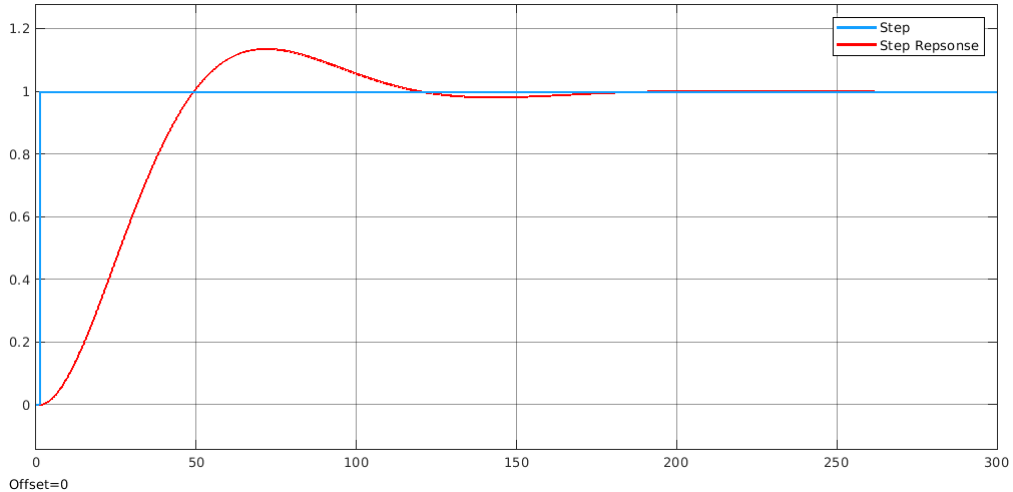


Figure 7.3: Corrected root locus of first order system

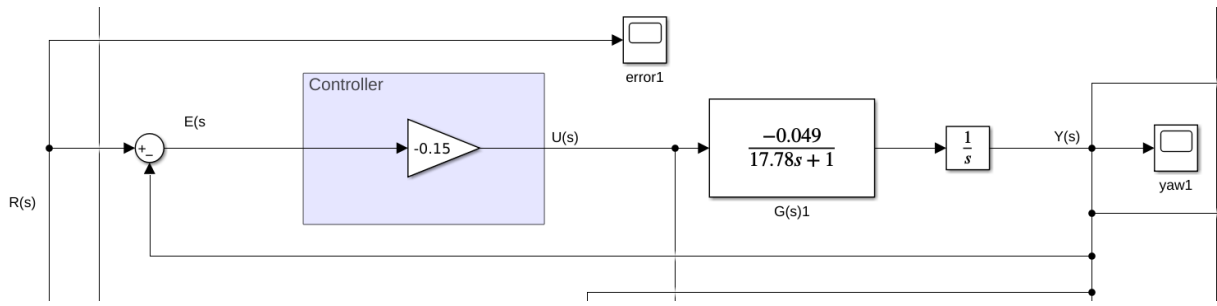
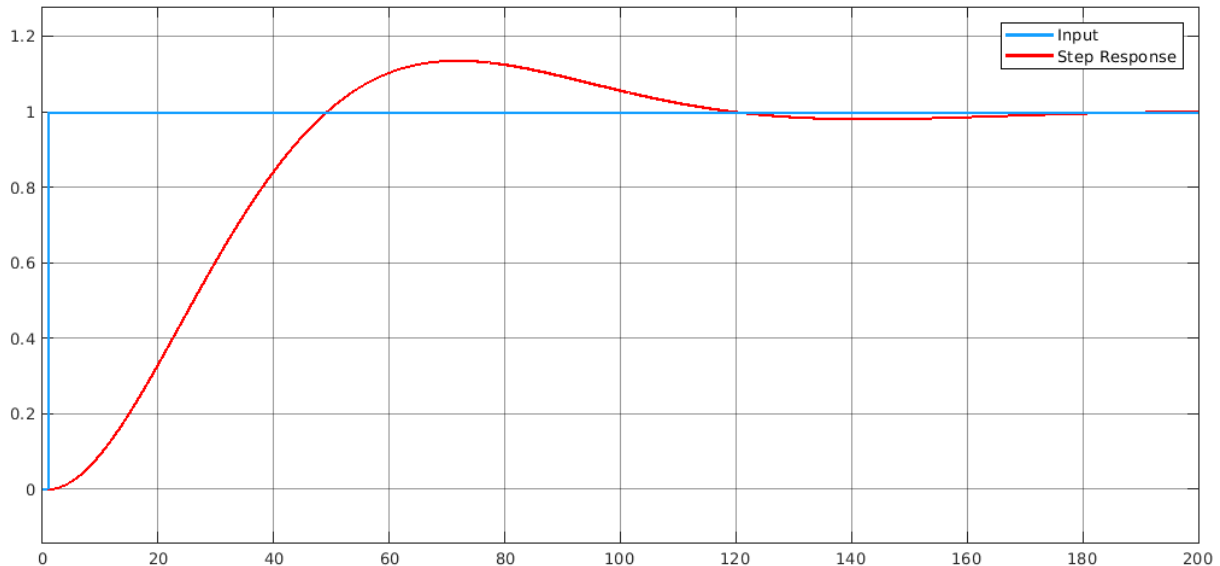
The bode plot is illustrated in Figure 7.4, the Phase Margin(PM) is $PM = 55$ and the Gain Margin(GM) $GM = 91.2dB$.

**Figure 7.4:** Bode plot

The step response of the system, illustrated in Figure 7.5 with a $k = 1$ shows that the system is underdamped. The time specifications, namely the rise time is $t_r = 34.29s$, the settling time is $t_s = 135.33s$ and maximum overshoot is $M_p = 0.118$.

**Figure 7.5:** Step response of first order system

The system was implemented in Simulink and is illustrated in Figure 7.6. The closed-loop step response of the system, illustrated in Figure 7.7.

**Figure 7.6:** Simulink model of system**Figure 7.7:** Closed loop step response

The controller used in this system is a Proportional(P) controller. The continuous controller is shown below,

$$D(s) = -K \quad (7.11)$$

To implement a continuous controller it has to be converted to a discrete controller. The discrete controller is simply the negative gain

$$D(z) = -K \quad (7.12)$$

Implementing the controller in the fourth order transfer function results in the following response,

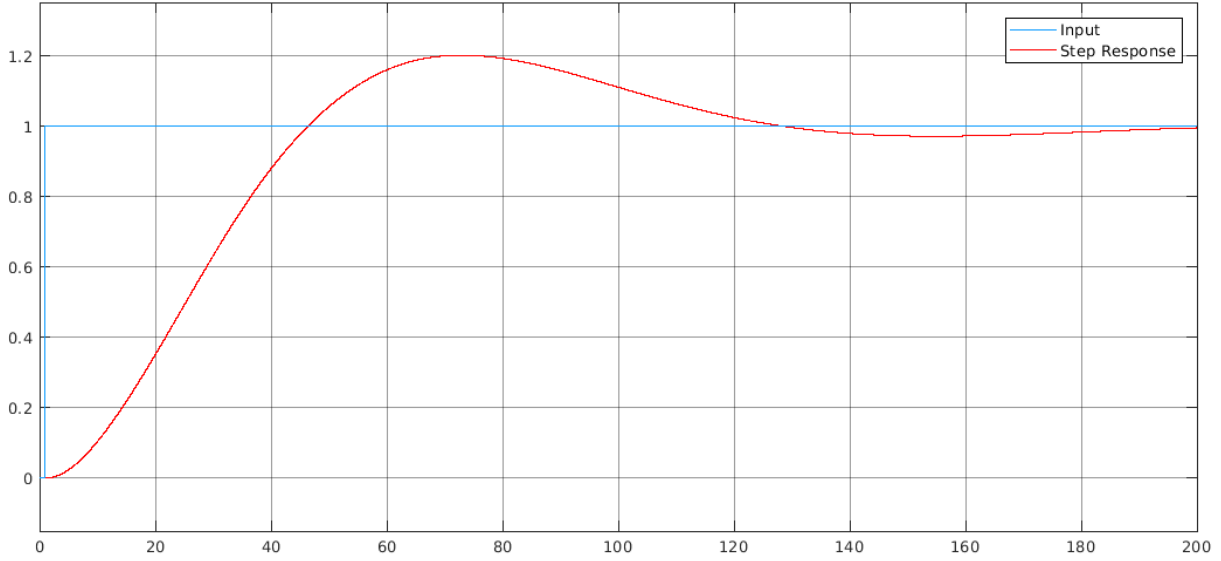


Figure 7.8: Implementation of controller in fourth order transfer function

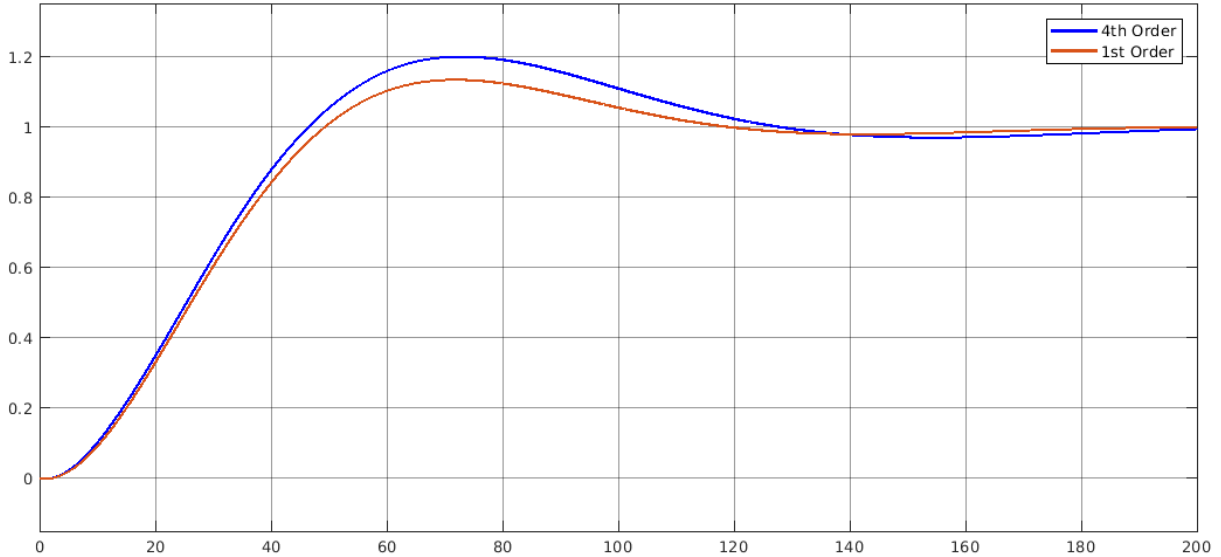


Figure 7.9: Comparison between 1st order and 4th order step responses

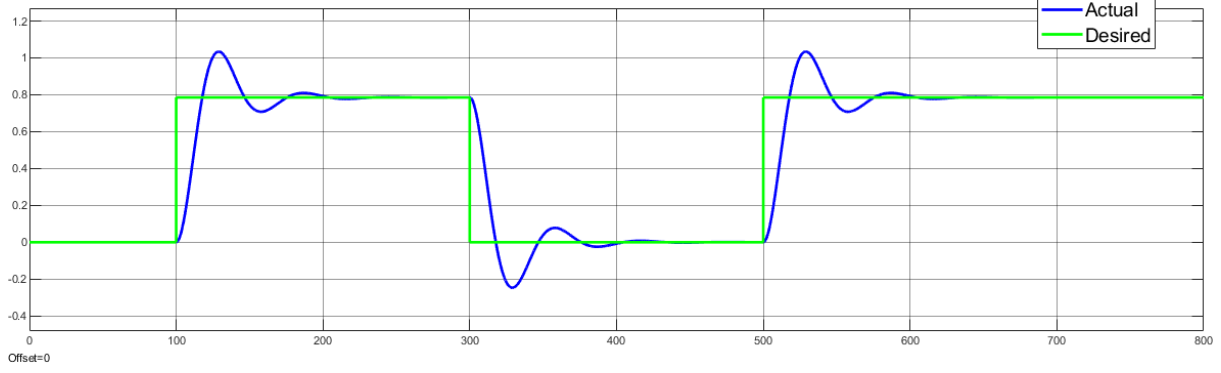
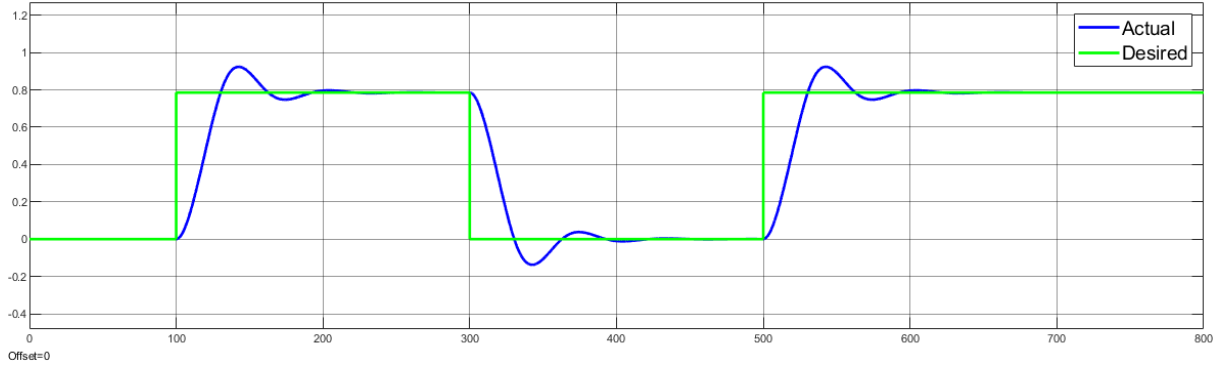
7.1.2. Non-Linear Rudder Control

The linear rudder controller implemented in Section 7.1.1, known as a Proportional Controller, tends to overshoot a lot in large changes in heading angle. The actual and desired heading of a linear controller is illustrated in Figure 7.10 and the non-linear controller illustrated in Figure 7.11. The non-linear controller is shown below,

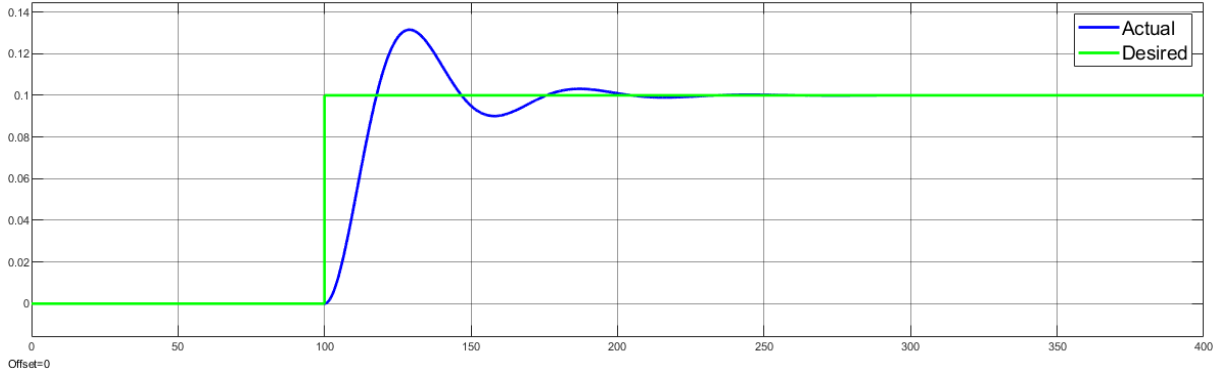
$$k(e) = \frac{k_p}{1 + c_p|e|} \quad (7.13)$$

for some $k_p, c_p > 0$ and hence sets the rudder command to

$$\delta = \delta_{NL}(e) = k(e)e \quad (7.14)$$

**Figure 7.10:** Linear control of heading**Figure 7.11:** Non-Linear control of heading

The benefit to using the non-linear controller compared to the linear controller is due to a more damped system when it comes to large heading changes. The smaller the heading error the more the non-linear controller will perform the same as the linear controller, as illustrated above. The linear controller tends to overshoot illustrated in Figure 7.10 and the non-linear controller has less of a overshoot Figure 7.11. The overshoots observed in Figure 7.12 and in Figure 7.13 is almost the same, having a error of around 3% of the step size compared with the overshoot observed in the case of a large heading change with is closer to a 17.5% overshoot.

**Figure 7.12:** Linear control of heading

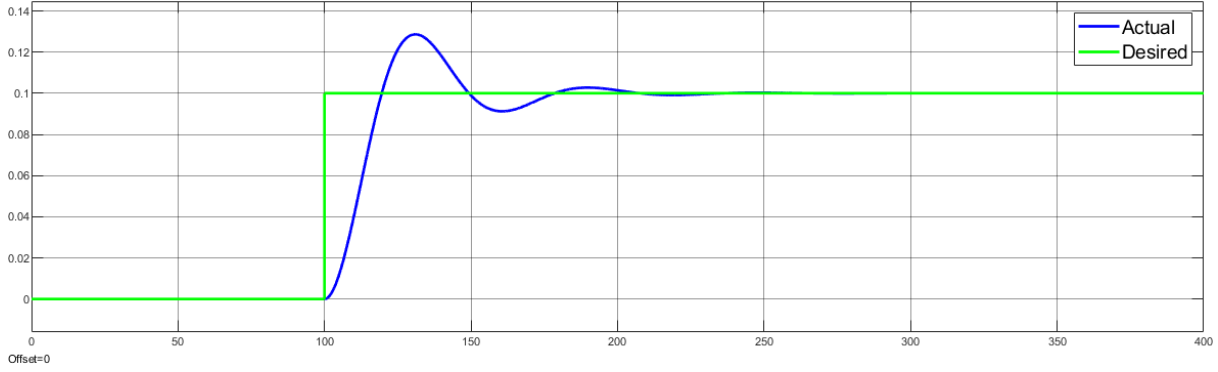


Figure 7.13: Non-Linear control of heading

7.2. Ocean Vessel Propulsion Control

The only propulsion source for sailboats are the wind. To propel the sailboat forward the sail needs to be aligned such that it catches the wind at the right angle. Firstly the reference angles need to be assigned. An example of a sailboat's sail angle is illustrated in Figure 7.1. The sail force is defined in [22], the article assumed a four degree of freedom model for the sailboat, surge sway heave and roll. The vector n was derived as

$$n = \begin{bmatrix} \dot{x} \\ \dot{y} \\ \dot{\psi} \\ \dot{\phi} \end{bmatrix} = \begin{bmatrix} u \cos(\psi) - v \sin(\psi) \cos(\phi) \\ u \sin(\psi) - v \cos(\psi) \cos(\phi) \\ r \cos(\phi) \\ p \end{bmatrix} \quad (7.15)$$

The apparent wind velocity will only be considered in the (x_b, y_b) plane. This results in the following definitions for apparent wind and velocity, which is defined as the wind experienced by the sailboat,

$$\psi_{aw} = \text{atan2}(V_{aw}^{yb}, V_{aw}^{xb}) = 2\text{atan}\left(\frac{V_{aw}^{yb}}{\sqrt{(V_{aw}^{yb})^2 + (V_{aw}^{xb})^2} + V_{aw}^{xb}}\right) \quad (7.16)$$

$$v_{aw} = \|V_{aw}^{b-frame}\| = \sqrt{(V_{aw}^{xb})^2 + (V_{aw}^{yb})^2} \quad (7.17)$$

The described force F_s define in Figure 7.1, can be represented in the vectorial representation of the aerodynamic force vector F_s into (x_b, y_b) plane is,

$$F_s = \begin{bmatrix} f_s \sin(\delta_s) \\ -f_s \cos(\delta_s) \cos(\phi) \end{bmatrix} \quad (7.18)$$

with $f_s = \|F_s\|$. The angle of attack on the sail is determined by the direction of the apparent wind vector V_{aw} and the sail angle, which is equal to

$$AoA = \pi - (\delta_s - \psi_{aw}) \quad (7.19)$$

The force generated by sail was discussed in Chapter 4, the force can be simplified in the surge direction as,

$$f_s = Kv_{aw}^2 \sin(\delta_s - \psi_{aw}) \sin(\delta_s) \quad (7.20)$$

where K is a constant value dependent on the physical dimensions of the sail, δ_s is the sail angle and v_{aw} is the apparent wind velocity.

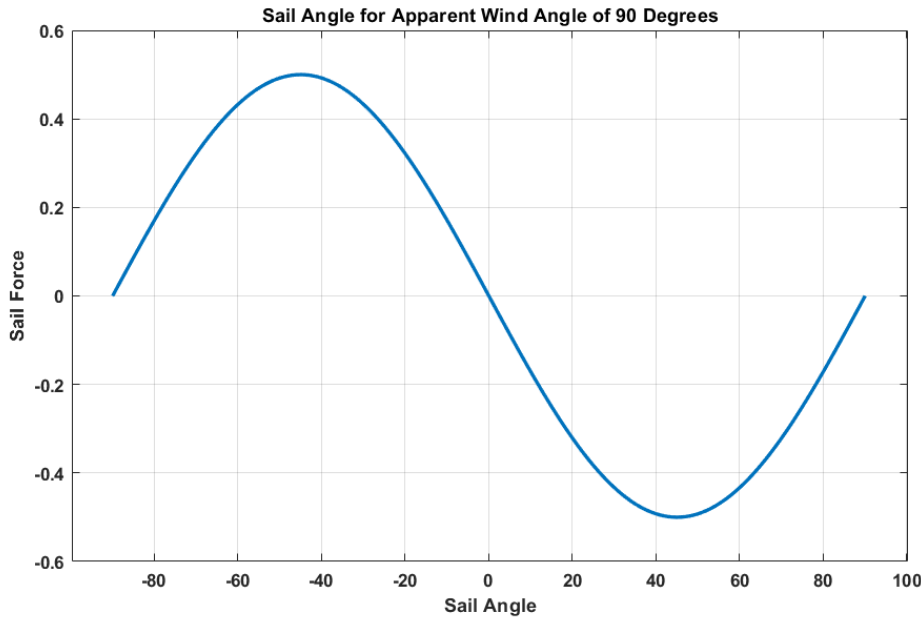


Figure 7.14: Sail Angle for Apparent wind angle of 90°

The control techniques for a sail was discussed in Chapter 2.2.2. The majority of control techniques are based on some look-up table form, where for a specific Apparent Wind Angle(AWA) a specific sail angle is used to generate the maximum sail force. Figure 7.14 illustrates the sail force in the surge direction, while varying the sail angle. The figure clearly shows that the sail will generate a positive force while it maintains a negative sail angle. The limitations imposed on the sail is that it will never open further than 90° in either directions and that it cannot abruptly changes its angle. The optimal sail angle was calculated for every wind angle and is shown in Table A.3. The calculated optimal sail angle when limiting the sail to $-90 < \delta_s < 90$, results in a straight line illustrated in Figure 7.15.

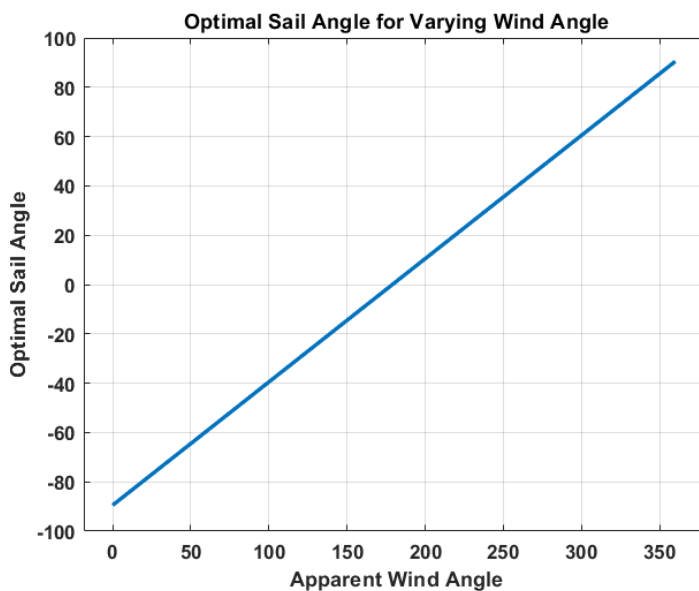


Figure 7.15: Optimal sail angle for varying wind angle

The straight line equation is represented by the following equation,

$$\delta_s = -0.5\lambda_\omega - 90 \quad (7.21)$$

This equation can be used to always set the sail angle to the optimal angle. There is however more limitations to consider. A sailboat cannot sail upwind. The zone wherein a sailboat cannot directly sail into the wind will be defined as the no-go zone. The sailboat is however possible to perform a maneuvering tactic called tacking that will allow it to follow a heading upwind while not sailing upwind. The sail force for AWA -180, -90, 0 and 90 is illustrated in Figure 7.16. When sailing upwind the AWA = 0 and sailing downwind the AWA = -180. The sail will generate a force, $f_s > 0$ for downwind sailing and $f_s < 0$ for upwind sailing for any δ_s .

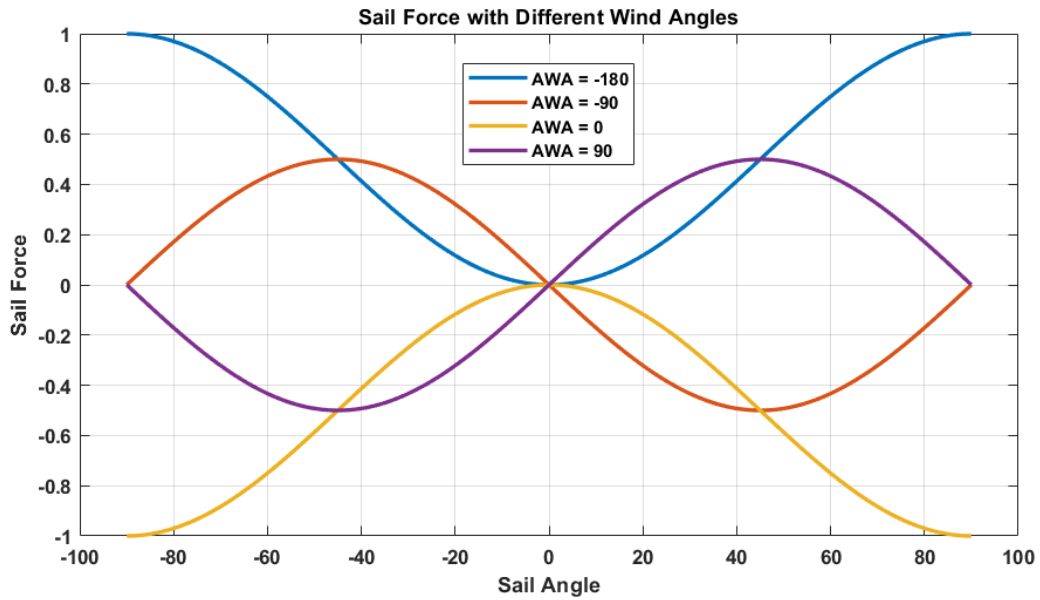


Figure 7.16: Sail force for specific apparent wind angles

7.3. Maneuverability Control

Generally the sailboat sail speed is illustrated with a polar diagram. Such a polar diagram is illustrated in Figure 7.17. The AWA is 0° , the polar plot clearly shows that the sailboat cannot sail into the region of $-30 < \psi < 30$. This is the previous mentioned no-go zone. The no-go zone, alongside a sail angle for optimise sailing, is illustrated as the gray area in Figure 7.18.

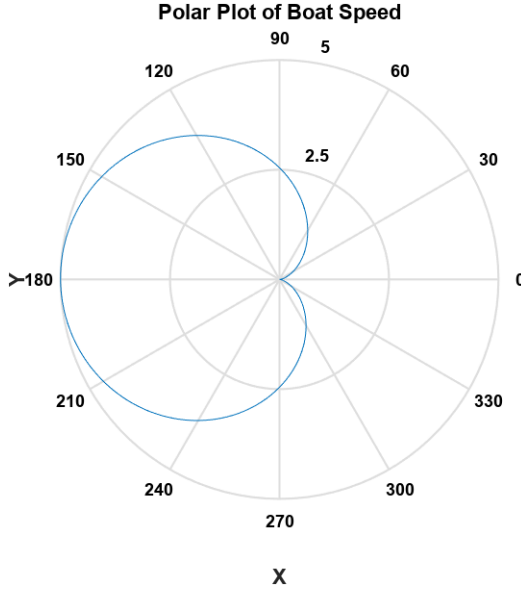


Figure 7.17: Boat Speed with a AWV of 5 km.s^{-1}

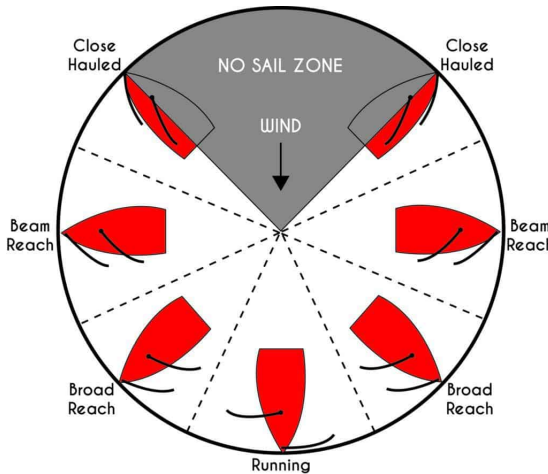


Figure 7.18: No-go zone

Sailing upwind is not possible but it is possible to sail in the upwind direction by form of tacking. A mathematical model for the tacking maneuver was developed in [23]. Tacking is when the sailboat is sailing close hauled, which is the definition for sailing close to the no sail zone, and then switching between a positive and negative heading into the wind. Figure 7.19 illustrates the maneuvering a sailboat will exercises when tacking.

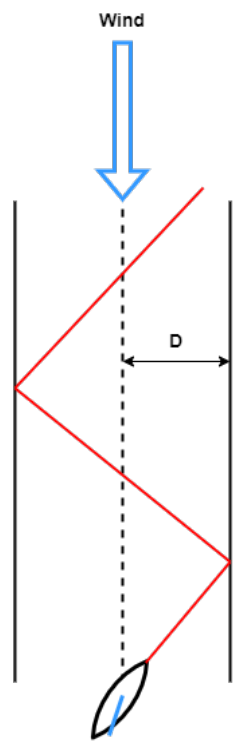


Figure 7.19: Tacking

The sail tacking maneuvering technique used is to set up a corridor

Bibliography

- [1] G. Kilpin, “Modelling and design of an autonomous sailboat for ocean observation,” Master’s thesis, University of Cape Town, Rondebosch, Cape Town, 7700, Sep. 2014.
- [2] M. Tranzatto, “Navigation and control for an autonomous sailing model boat,” Master’s thesis, University of Pisa, Lungarno Pacinotti 43, Italy, Sep. 2016.
- [3] K. L. Wille, “Autonomous sailboats,” Master’s thesis, Norwegian University of Science and Technology, Trondheim Ålesund Gjøvik, Norway, Jun. 2016.
- [4] Y.-W. C. J. W. S.-Y. C. Yee-Teng Ang, Wey-Kean Ng and L. B. Firth, “An autonomous sailboat for environment monitoring,” *Thirteenth International Conference on Ubiquitous and Future Networks*, pp. 242–246, 2022.
- [5] M. A.-C. W. S. R. D. W. Joga Dharma Setiawan, Deddy Chrismianto and S. Alimi, “Development of dynamic model of autonomous sailboat for simulation and control,” *International Conference on Information Technology, Computer and Electrical Engineering*, no. 7, pp. 52–57, 2020.
- [6] Saildrone, “About us,” <https://www.saildrone.com/about>, 2023.
- [7] K. D. Do and J. Pan, *Control of Ships and Underwater Vehicles*. Springer Science+Business Media, LLC, 2009.
- [8] R. Featherstone, *Rigid Body Dynamics Algorithms*. Springer Science+Business Media, LLC, 2008.
- [9] O. M. Faltinsen, *Sea Loads on Ships and Offshore Structures*. Cambridge University Press, 1990.
- [10] W. Blödnermann, “Parameter identification of wind loads on ships,” *Journal of Wind Engineering and Industrial Aerodynamics*, vol. 51, no. 3, pp. 339–351, 1994.
- [11] S. Buckles, “The ultimate guide to sail types and rigs,” *Sailing Guides*, 2023.
- [12] C. Tretow, “Design of a free-rotating wing sail for an autonomous sailboat,” Master’s thesis, KTH ROYAL INSTITUTE OF TECHNOLOGY SCHOOL OF ENGINEERING SCIENCES, Teknikringen 8D, 114 28 Stockholm, Sweden, Sep. 2017.
- [13] A. F. Molland and S. R. Turnock, *Marine Rudder and Control Surface*. Butterworth-Heinemann, 2021.
- [14] K. Legursky, “System identification and the modeling of sailing yachts,” Ph.D. dissertation, University of Kansas, 2013.
- [15] D. Morris, “Derivation of forces on a sail using pressure and shape measurements at full-scale,” Master’s thesis, CHALMERS UNIVERSITY OF TECHNOLOGY, Chalmersplatsen 4, 412 96 Göteborg, Sweden, Sep. 2011.
- [16] L. Larsson and R. E. Eliasson, *Principles of Yacht Design*. International Marine/McGraw-Hill, 2007.
- [17] A. Gentry, “The aerodynamics of sail interaction,” *AIAA Symposium on the Aero/Hydronautics of Sailing*, vol. 1, no. 1, p. 8, 1971.

- [18] Y. Masuyama and T. Fukasawa, “Tacking simulation of sailing yachts with new model of aerodynamic force variation during tacking maneuver,” *Journal of Sailboat Technology*, vol. 1, no. 1, pp. 1–34, 2011.
- [19] J. A. A. Engelbrecht, “Advance automation 833: Introductory course to aircraft dynamics,” April 2019, aircrafts.
- [20] L. E. Dubins, “On curves of minimal length with a constraint on average curvature, and with prescribed initial and terminal positions and tangents,” *American Journal of Mathematics*, vol. 79, no. 3, pp. 497–516, 1957.
- [21] M. Breivik and T. I. Fossen, “Path following for marine surface vessels,” *Centre for Ships and Ocean Structures (CESOS*, no. 1, pp. 2282–2289, 2004.
- [22] S. N. H. Abrougui and H. Dallagi, “Modeling and autopilot design for an autonomous catamaran sailboat based on feedback linearization,” *International Conference on Advanced Systems and Emergent Technologies*, vol. 1, no. 1, pp. 130–135, 2019.
- [23] K. J. V. E. J. de Ridder and J. A. Keuning, “A mathematical model for the tacking maneuver of a sailing yacht,” *The International HISWA Symposium on Yacht Design and Yacht Construction 2004*, no. 1, pp. 1–33, 2004.

Appendix A

Additional Modelling Information

A.1. Notation and Vector Definitions

Table A.1: SNAME Notation for ocean vessels

Degree of freedom		Force and moment	Linear and angular velocity	Position and Euler angles
1	Surge	X	u	x
2	Sway	Y	v	y
3	Heave	Z	w	z
4	Roll	K	p	ϕ
5	Pitch	M	q	θ
6	Yaw	N	r	ψ

Table A.2: Rigid body motion vectors

Vector	Components	Definition
\mathbf{f}_{Ob}	$[X \ Y \ Z]^T$	force decomposed in the body-fixed frame
\mathbf{m}_{Ob}	$[K \ M \ N]^T$	moment decomposed in the body-fixed frame
\mathbf{v}_{Ob}	$[u \ v \ w]^T$	linear velocity decomposed in the body-fixed frame
\mathbf{w}_{Ob}^E	$[p \ q \ r]^T$	angular velocity of the body-fixed relative to the earth-fixed frame
\mathbf{r}_{Ob}	$[x_g \ y_g \ z_g]^T$	vector from O_b to CG decomposed in the body-fixed frame

A.2. Modeling Equations

$$\mathbf{M}_{\mathbf{RB}} = \begin{bmatrix} m & 0 & 0 & mz_g & mz_g & -my_g \\ 0 & m & 0 & 0 & 0 & mx_g \\ 0 & 0 & m & -mx_g & -mx_g & 0 \\ 0 & -mz_g & -my_g & I_x & -I_{xy} & -I_{xz} \\ mz_g & 0 & -mx_g & -I_{xy} & I_y & -I_y z \\ -my_g & mx_g & 0 & -I_{zx} & -I_{zy} & I_z \end{bmatrix} \quad (\text{A.1})$$

$$\mathbf{C}_{\mathbf{RB}}(\mathbf{v}) = \begin{bmatrix} 0 & 0 & 0 & m(y_g q + z_g r) & -m(x_g q - w) & -m(x_g r + v) \\ 0 & 0 & 0 & -m(y_g p + w) & m(z_g r + x_g p) & -m(y_g r - u) \\ 0 & 0 & 0 & -m(z_g p - v) & -m(z_g q + u) & m(x_g p + y_g q) \\ -m(y_g q + z_g r) & m(y_g p + w) & m(y_g p - v) & 0 & -I_{yz} q - I_{xz} q + I_z r & I_{yz} r + I_{xy} p - I_y q \\ m(x_g p - w) & -m(z_g r - x_g p) & m(z_g q + u) & I_{yz} q + I_{xz} p - I_z r & 0 & -I_{xz} r - I_{xy} q + I_X p \\ m(x_g r + v) & m(y_g r - u) & -m(x_g p + y_g q) & -I_{yz} r - I_{xy} p + I_y q & I_{xz} r + I_{xy} q - I_x p & 0 \end{bmatrix} \quad (\text{A.2})$$

$$a_1 = X_{\dot{u}} u + X_{\dot{v}} v + X_{\dot{w}} w + X_{\dot{p}} p + X_{\dot{q}} q + X_{\dot{r}} r \quad (\text{A.3})$$

$$a_2 = Y_{\dot{u}} u + Y_{\dot{v}} v + Y_{\dot{w}} w + Y_{\dot{p}} p + Y_{\dot{q}} q + Y_{\dot{r}} r \quad (\text{A.4})$$

$$a_3 = Z_{\dot{u}} u + Z_{\dot{v}} v + Z_{\dot{w}} w + Z_{\dot{p}} p + Z_{\dot{q}} q + Z_{\dot{r}} r \quad (\text{A.5})$$

$$b_1 = K_{\dot{u}} u + K_{\dot{v}} v + K_{\dot{w}} w + K_{\dot{p}} p + K_{\dot{q}} q + K_{\dot{r}} r \quad (\text{A.6})$$

$$b_2 = M_{\dot{u}} u + M_{\dot{v}} v + M_{\dot{w}} w + M_{\dot{p}} p + M_{\dot{q}} q + M_{\dot{r}} r \quad (\text{A.7})$$

$$b_3 = N_{\dot{u}} u + N_{\dot{v}} v + N_{\dot{w}} w + N_{\dot{p}} p + N_{\dot{q}} q + N_{\dot{r}} r \quad (\text{A.8})$$

Table A.3: Sail Angle Look-up Table

Apparent Wind Angle	Sail Angle	Apparent Wind Angle	Sail Angle
0	-90	1	-89
2	-89	3	-88
4	-89	5	-87
6	-88	7	-86
8	-87	9	-85
10	-86	11	-84
12	-85	13	-83
14	-84	15	-82
16	-83	17	-81
18	-82	19	-80
20	-81	21	-79
22	-80	23	-78
24	-79	25	-77
26	-78	27	-76
28	-77	29	-75
30	-76	31	-74
...
330	75	331	76
332	76	333	77
334	77	335	78
336	78	337	79
338	79	339	80
340	80	341	81
342	81	343	82
344	82	345	83
346	83	347	84
348	84	349	85
350	85	351	86
352	86	353	87
354	87	355	88
356	88	357	89
358	89	359	90